land

MDPI

*Article*

# An Overview of the Geomorphological Characteristics of the Pergamon Micro-Region (Bakırçay and Madra River Catchments, Aegean Region, West Turkey)

**Xun Yang [1,*], Fabian Becker [1], Daniel Knitter [2] and Brigitta Schütt [1]**

[1] Physical Geography, Institute of Geographical Sciences, Freie Universität Berlin, Malteserstraße 74-100, 12249 Berlin, Germany; fabian.becker@fu-berlin.de (F.B.); Brigitta.Schuett@fu-berlin.de (B.S.)
[2] Physical Geography, Department of Geography, Christian-Albrechts-Universität zu Kiel, Ludewig-Meyn-Straße 14, 24118 Kiel, Germany; knitter@geographie.uni-kiel.de
* Correspondence: xun.yang@fu-berlin.de

**Abstract:** Current landforms are the basis for understanding past geomorphodynamics and human activities. Based on multiple materials and methods, including geomorphometric analyses of a digital elevation model and visual interpretations of satellite images, different landscape units of the Bakırçay and Madra River catchments in the environs of ancient Pergamon are described. The area was mainly shaped by tectonics that formed a horst-and-graben structure; small Miocene horsts and NE-trending subgrabens in the Kozak and Yunt Dağı Mountains were separated by the NEE-trending Plio-Pleistocene Bergama Graben. The asymmetry in relief, drainage network, and sediment accumulation between the Kozak Mountains to the north and the Yunt Dağı Mountains to the south of the lower Bakırçay plain characterize the Pergamon Micro-Region. The regional relief characteristics, with wide flat basin and plateau areas, are suitable for agriculture. Complemented by its richness in natural resources, the Pergamon Micro-Region became a preferred settlement area, with evidence of human impact since the Hellenistic–Roman period at the latest. As a consequence of settlement activities, several landscape engineering measures were implemented simultaneously with a parallel change in morphodynamics.

**Keywords:** geomorphological map; geomorphometry; geomorphodynamics; human–environment interaction



**Citation:** Yang, X.; Becker, F.; Knitter, D.; Schütt, B. An Overview of the Geomorphological Characteristics of the Pergamon Micro-Region (Bakırçay and Madra River Catchments, Aegean Region, West Turkey). *Land* **2021**, *10*, 667. https://doi.org/10.3390/land10070667

Academic Editor: Oren Ackermann

Received: 14 May 2021
Accepted: 21 June 2021
Published: 24 June 2021



## 1. Introduction

The Aegean Region of Turkey (Ege Bölümü) is characterized by a number of mountain ranges below ca. 2500 m a.s.l. that are dissected by several large east–west oriented valleys (Figure 1B) [1]. Sediments transported and deposited by rivers caused the development of alluvial plains and large prograding deltas [1–3]. Abundant prehistoric and historic settlements were built on and along these valleys and deltas; for example, Troy in the Karamenderes valley [4–7]; Pergamon and its rural settlements in the Bakırçay valley [8–12]; Phocaea and Smyrna at the former mouth of the Gediz River [5]; Ephesus in the Kücük Menderes valley [5,13–15]; and Miletus in the Büyük Menderes valley [5,12,16].

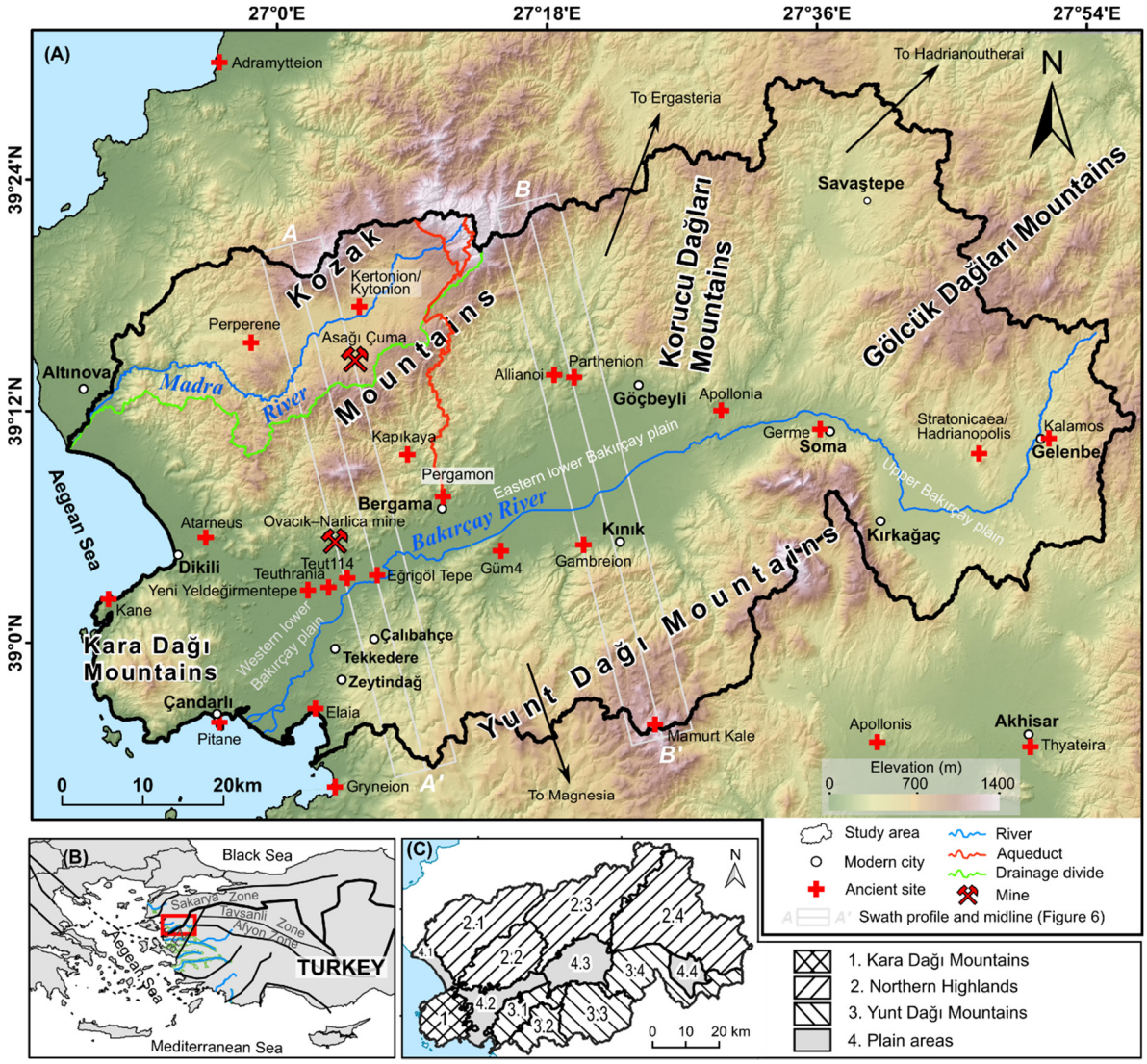


**Figure 1.** (**A**) Overview map of the Pergamon Micro-Region (Bakırçay and Madra River catchments and the adjacent coastal areas). Data: (1) ancient site [9–11,17–19]; (2) aqueduct: The Atlas Project of Roman Aqueducts (https://www.romaq.org/the-project/aqueducts/article/692#tab-details, last accessed 8 June 2021) [20] (p. 150); (3) mine site [21,22]; (4) elevation data: TanDEM-X digital elevation model (12-m horizontal resolution) [23,24]. (**B**) The location of the study area (red rectangle), highlighted with the major westward-trending rivers (blue lines) and their alluvial plains (green polygons) along the Aegean coastal region of west Turkey (modified from [1]), and the major tectonic structures (shown as black thin lines in the west of Anatolia and dashed lines linked to the sutures across the Aegean Sea) and tectonic zones (black thick line: the İzmir–Ankara Suture Zone; BFZ: Bornova Flysch Zone) modified from [25]). (**C**) Geomorphological units and subunits of the Pergamon Micro-Region.

The current study focuses on one of these valleys, the Bakırçay valley, which is directly related to the Pergamon Micro-Region. This microregion has been settled at least since the Neolithic period [26]. The site of Pergamon, on the hilltop northeast of modern Bergama (Figure 1A), had already become a polis by the fourth century BC and then became the capital of the Kingdom of Pergamon in 281–133 BC. Pergamon doubled its size prior to the beginning of the third century and subsequently the decline had already set in [27,28]. The Hellenistic–Roman urban center of Pergamon (a UNESCO World Heritage site) and its micro-region have been intensively studied, predominantly from the archaeological point of view, since the end of the 19th century [27,29–34]. More recently, geoarchaeological research has been integrated, focusing on selected archaeological sites and related subbasins

along the western lower Bakırçay plain [8–11,35–42] and the neighboring Madra River delta [43].

The majority of prehistoric and ancient settlements in the Pergamon Micro-Region were located in the transitional areas between the mountains and alluvial plains or along flat unconfined valleys (Figure 1A) [9–11,17–19]. These areas appear to be particularly suitable for the foundation of human settlements and for local supplies and route networks. They are relatively flood-protected, adjacent to fertile plains for agriculture and to mountainous hinterland for horticulture and pastoralism [9,17,18]. Examples include the Greek polis Atarneus (from the sixth to the fourth century BC) in the southwestern Kozak Mountains [8,9] and the Late Chalcolithic/Byzantine settlement Güm4 in the northern Yunt Dağı Mountains (Figure 1A) [18,19]. However, some of the original flood-safe areas became prone to flooding because of continuous aggradation of the lower Bakırçay plain and occasionally flood episodes, e.g., the site Teut114 after the 1st century CE [10] and the Late Chalcolithic-to-Bronze Age settlement Yeni Yeldeğirmentepe [11] in the western lower Bakırçay plain. In addition to the settlements adjacent to the main Bakırçay alluvial plain, prehistoric sites were located on or close to the coast during the Middle Holocene, when alluvial and colluvial conditions began to dominate the littoral areas [1]. The settlements on the Madra River delta and around the Bakırçay River delta are prominent examples [36,38,43]. Flourishing in a sheltered position, the Greco-Roman harbor city of Elaia (Figure 1A) avoided the presumably high sedimentation of the Bakırçay River [36,38]. Several ancient human settlements and archaeological remains have been documented in the mountains adjoining the lower Bakırçay plain [17,31,44], which, however, lack systematic geoarchaeological research.

Previous geomorphological and sedimentological studies indicate not only the environmental potential for human activities, but also the Holocene local morphodynamics in the western lower Bakırçay plain and the adjacent piedmonts. Moreover, a meta-analysis of the $^{14}$C-ages from site-related sediment sequences reconstructed several phases of increased geomorphodynamics during the Holocene, which are presumably related to multiple triggers, such as climate, population dynamics, and local settlement history [42].

Large spatial-scale geological studies in western Anatolia—regarding the Miocene-Quaternary grabens and their deposits [45–48], Miocene volcanism [49,50], and river responses to Quaternary tectonics [1,25,51]—indicate a complex tectonic-dominated landscape of uplands (mainly as horsts) and plains (mainly as grabens).

The morphological complexity of a landscape in a catchment subsequently influences the sediment connectivity [52]. Landscape configuration controls where and how long the sediments are stored [53,54]. Wider valleys have larger accommodation spaces for sediments to be stored within the catchment and less in the basin outlet [54], which could promote landscape stability. Combined factors of neotectonics [48], cycles of climate [55] and sea level changes [1,39], vegetation degradation, and increased human activities [40,42] are able to increase sediment and landscape dynamics [53,54] and consequently shape the local geomorphology [56,57].

An identification of geomorphological characteristics forms the basis for a reconstruction of geomorphodynamics, which allows insights to be gained into the distribution of human activities in a landscape, including ancient human settlements and route networks. Despite the previously mentioned site-related geoarchaeological, regional, and supra-regional geological and paleoenvironmental studies, geomorphological characterizations of the Bakırçay and Madra River catchments in the environs of ancient Pergamon are currently lacking. Therefore, our main objectives are (a) to provide a catchment-scale overview and (sub)unit comparison of current landforms in the Bakırçay and Madra River catchments based on geomorphological mapping and geomorphometric analyses; and (b) to assess potential drivers of landscape dynamics and to infer the consequences for different landscape units. On this basis, the attractiveness and appropriateness of the Pergamon Micro-Region as a preferred settlement area since Hellenistic times are sketched.

## 2. Natural Characteristics of the Pergamon Micro-Region

### *2.1. Geographical Setting*

The study area comprises the Bakırçay River catchment (ca. 3382 km$^2$) and the neighboring Madra River catchment (ca. 382 km$^2$), and the adjacent coastal areas along the Aegean Sea (Figure 1A). It includes a major part of the Pergamon Micro-Region [28], where important natural resources (such as stone as a building material, clay for ceramic production, soil for agricultural production, and water as a daily necessity) have been utilized to supply the city of Pergamon [17,43,58]. Located between 38°54′–39°29′ N and 26°48′–27°57′ E, this area extends approximately 100 km in the E–W direction and 66 km in the N–S direction, covering an area of ca. 4124 km$^2$.

To the north, the divide between the Bakırçay and Madra River catchments (Figure 1A) runs along the southern range of the Kozak Mountains [37,51,59] (in other studies, the mountains are also mentioned as Mount Kozak [45], Madra Mountain [43], Madra Dağı [17,48], or Pindasos [28]), the Korucu Dağları Mountains, and the Gölcük Dağları Mountains [60]. To the south, the divide of the Bakırçay River runs along the northern range of the Yunt Dağı Mountains (Figure 1A) (i.e., Yüntdağ Mountains [36,45], Yuntdağ Mountain Complex [38], Yunt Mountains [48], Yund Dağı [17], or Aspordenon [28]). The Kara Dağı Mountains (i.e., Kara Dağ massif [9] or Dikili–Çandarlı high [49]) on the Kane Peninsula [17] are located west of the Bakırçay plain [38].

The Bakırçay River (the ancient Kaïkos) is one of the E–W oriented graben-related rivers of the Aegean Region in Turkey [5,61–63] (Figure 1B). It originates from the Kocadağ (in the Gölcük Dağları Mountains; Figure 1A). After flowing through the upper and the (eastern and western) lower Bakırçay alluvial plain, it enters into the Aegean Sea and develops a delta between Zeytindağ (west Yunt Dağı Mountains) and Çandarlı (south Kara Dağı Mountains) (Figure 1A). Its natural channel pattern changes from braided in the middle reaches to meandering in its lower reaches [11,61]. The Madra River drains through the intramountainous basin of the Kozak interior plain and it incises the steep valley in the western Kozak Mountains (Figure 1A). After passing through the Altınova–Dikili littoral plain, deposits of the Madra River form a delta in the Aegean Sea [43], which is smaller than the Bakırçay delta.

### *2.2. Tectonics, Bedrock, and Soil*

Geologically, the study area belongs to the westward-drifting Aegean–Anatolian microplate [25,64], comprised by the Sakarya Zone in the north and the Bornova Flysch Zone in the south (Figure 1B) [25]. Among these continental zones is the NE-trending İzmir–Ankara Suture Zone (IASZ) (Figure 1B) [25,48]. NE-trending dextral strike slip faults of the North Anatolian Fault System and N–NW-trending extension of the Aegean Extensional System simultaneously controlled the tectonic structures in this area [48]. Several horsts and grabens formed under the tectonic paleostress, e.g., the Kozak Horst, the Miocene Zeytindağ and Örenli–Eğiller grabens, and the Plio-Pleistocene Bergama and Ayvalik–Lesvos grabens (Figure 2) [48,65,66]. The Bergama Graben continues to subside at an average rate less than 1 cm per 1000 years [39,61]. The tectonic stress caused severe earthquakes during the last two millennia, for example, the Çandarlı earthquake in 105 CE [67] (p. 54), the Dikili earthquake in 1939, and the Göçbeyli earthquake in 1919, the magnitudes of the latter two being $\geq$6.5 [68] (Figure 2). Within its western sector, several Miocene volcanic domes (Turkish *tepe*, hills) rise from the Bakırçay plain [50]. Faults are mainly found in three zones, viz., the Altınova–Dikili fault zone (Figure 2: ①), the Zeytindağ–Bergama fault zone (Figure 2: ②), and the Soma–Kırkağaç fault zone (Figure 2: ③) [69–72]. The latter two zones are dominated by normal faults that were active during the Holocene (Figure 2).

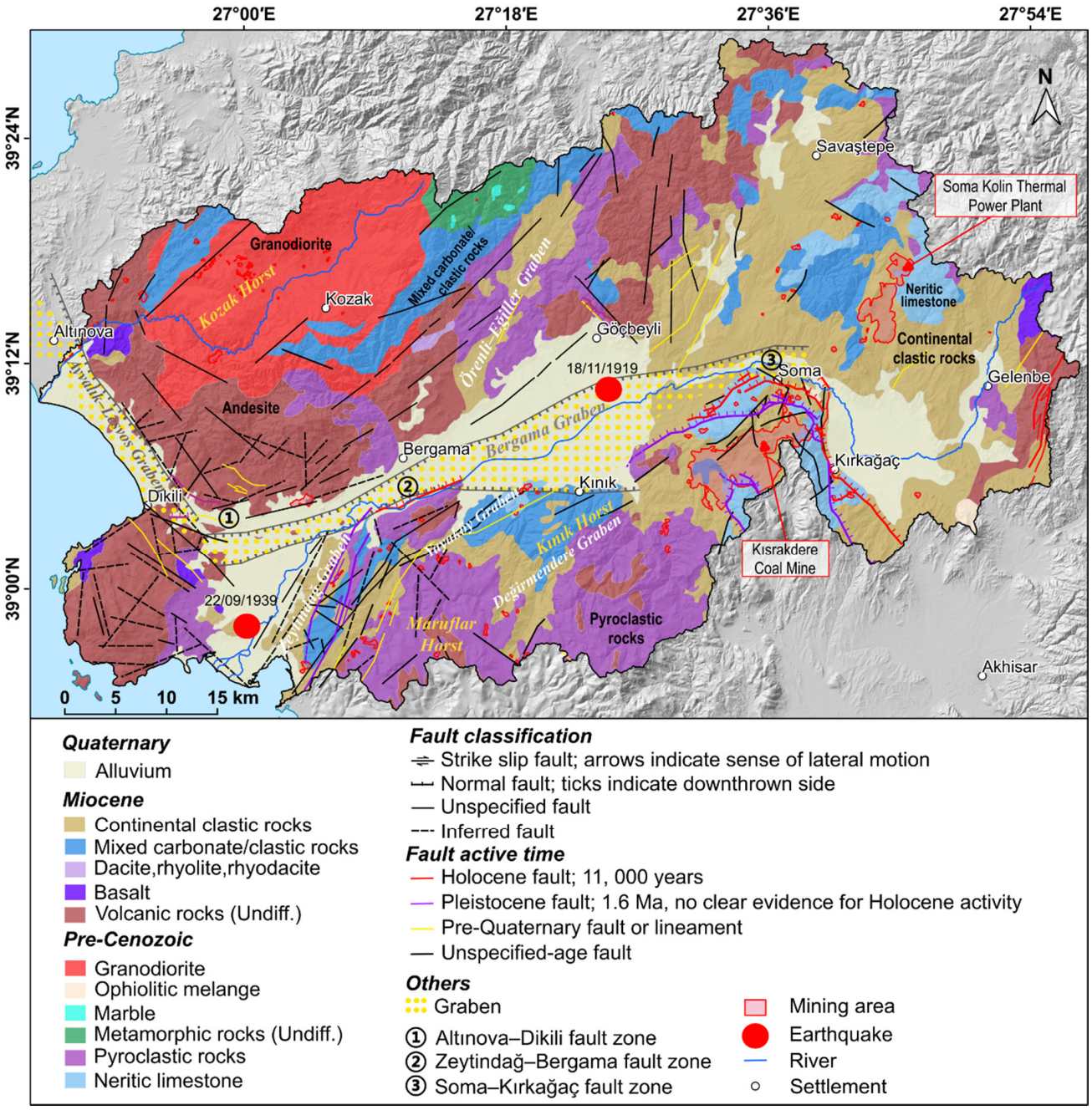


**Figure 2.** Geological map of the Bakırçay and Madra River catchments and their adjacent coastal areas. Data: (1) bedrock: Geological Map of Turkey, 1:500,000 (İzmir) [60]; (2) fault: 1:250,000 scale Turkey Active Fault Maps [69–72] and the unspecified-age fault (black line) [45,60,73]; (3) location of graben, horst, and fault zones [45]; (4) mining area: Google Earth satellite images (WorldView-2, last accessed 8 June 2020); (5) earthquake epicenter of $M \geq 6.5$ since 1900 [68].

Pre-Miocene granodioritic rocks form the core of the Kozak Mountains and are surrounded by Mesozoic metamorphic rocks, Miocene carbonate rocks, and volcanic formations [60] (Figure 2). The volcanic units are dominated by andesites, basalts, and pyroclastic rocks. The latter rock can also be found at the western Yunt Dağı Mountains, e.g., the Maruflar Horst (Figure 2). Miocene continental clastic rocks were deposited at the outer belt of the Kozak Horst, mostly covering the old carbonate rocks in the Gölcük Dağları Mountains and some at the depressions in the Yunt Dağı Mountains [60] (Figure 2).

The formation of different soils in this area mainly depends on lithology and vegetation cover [74]. The predominant soil types are Cambisols–Leptosols in the mountains and

Fluvisols in the alluvial plains [75,76]. Beyond these, brown forest soils, which dominantly formed on granodiorite parent materials, are the most common soil type in the Kozak Mountains; Rendzinas are mainly distributed on calcareous-rich sedimentary bedrocks [74]. In the area along Soma–Kırkağaç, Luvisols prevail [75,76].

### *2.3. Climate*

Located in the Aegean Region, the study area has a typical Mediterranean subhumid climate [77]. The area is characterized by dry and hot summers, and mild and wet winters ("Csa" climate according to the Köppen–Geiger classification [78]). Between 1981 and 2010, the annual temperature averaged 16.2 °C in Dikili and 14.7 °C in Bergama, and the annual precipitation averaged 711 mm in Dikili and 749 mm in Bergama (Figure 3). At both locations, most rain falls in December and January, reaching 140 mm per month; the dry period spans from May to October (Figure 3). The maximum precipitation recorded at the meteorological station in Dikili between 1939 and 1996 totaled 183 mm within 24 h [74].

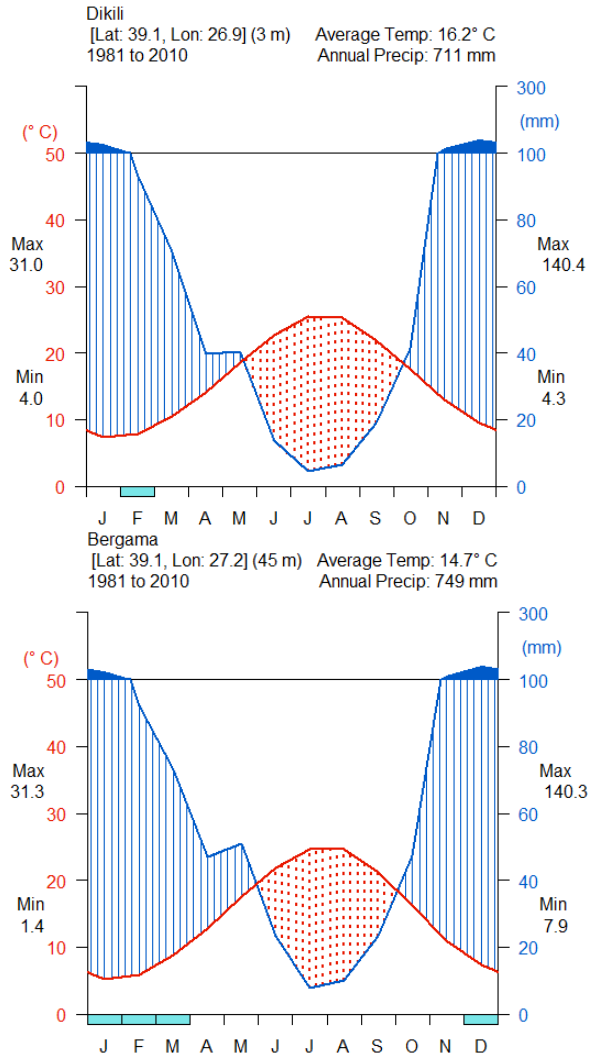


**Figure 3.** Climate diagrams of Dikili and Bergama (reference period: 1981–2010), showing Mediterranean subhumid climate with arid conditions prevailing during summer months and extreme rainfall during winter months. Data: Climatic Research Unit (CRU) (database: http://data.ceda.ac.uk/badc/cru/data/cru_ts/cru_ts_4.01/data, last accessed 8 November 2020) [79].

Between 9 and 3 ka BP, climate conditions in the eastern Mediterranean became gradually drier after the relatively wet early Holocene; the period between 6 and 3 ka BP appears to have been the driest period during the Holocene [55]. More rapid (centennial-

scale) climate change events were interspersed around 6.7–6.3 ka BP, 4.5–4.3 ka BP, and 3.5–3.3 ka BP in the Mediterranean [55]. During the past three millennia, the hydroclimate became slightly wetter [57]. Climate changes, particularly rapid climate change events, are assumed to be in chronological agreement with major archaeological turnover events in the Aegean/Levantine region [80].

### *2.4. Vegetation*

During the early Holocene (9500–8500 BP), the landscape ecology in the Mediterranean region remained stable, with the forest extent reaching a maximum [57]. The gradual decline in forest between 7500 and 3000 BP was impacted both by climate change and human activities; subsequently, the landscape has continued to be subject to anthropogenic pressure [57]. Now, the remnants of the natural vegetation cover have retreated to steep valley sites (Figure S6, Corine Land Cover data [81]), appearing predominantly as contracted vegetation [74].

Present-day vegetation cover in the study area is Thermo-Mediterranean [77] or Eu-Mediterranean-type [40]. Forest communities and shrub formations (woody shrubs with evergreen leaves: *maquis*, and xerophyte bushes and thorns: *garrigue*) of the Mediterranean region are widespread in the mountainous areas [3]. Dense forest (mainly coniferous forest) is dominant at elevations above 500 m a.s.l. at the outer belt of the Kozak intramountainous basin and the eastern Yunt Dağı Mountains (Figure S6). Stone pine forests (*Pinus pinea*) occur in the Kozak Mountains in elevations between 600 and 700 m a.s.l. [74]. Shrub and herbaceous vegetation associations are widespread in the Kara Dağı Mountains at 200 and 500 m a.s.l. The western slopes of the Kozak Mountains and the Maruflar Horst (in Yunt Dağı Mountains) are intensively used for grazing [9,43] (Figure S6). The Zeytindağ Graben (the western Yunt Dağı Mountains) and the margins of the upper Bakırçay plain (Soma–Kırkağaç area) are largely cultivated with olive trees (Figure S6). The common vegetation of the Bakırçay and Madra alluvial plains comprises cash crops, mainly cotton and vegetables [3,74]. Sporadically, crops are also cultivated in intramountainous basins and infilled valleys (Figure S6).

## 3. Materials and Methods

### *3.1. Survey of Geomorphological Features*

Major geomorphological features were mapped using QGIS 3.8 [82], supported by a literature review, field observations, visual interpretations of freely available high-resolution satellite images provided by Google Earth (<1 m resolution; DigitalGlobe, Inc., maps.google.com, last accessed 8 June 2020), and geomorphometric derivates from TanDEM-X data [23,24] (Section 3.2.). Their subdivisions with definition and classification rules are summarized in Table S1 [83]. The materials used for interpretation and field photos of each landform unit are provided in Supplementary Materials Figures S1–S7.

Rivers were digitized from topographic and geological maps [69–72]. Please note that the field observations were mainly conducted in the lower Bakırçay plain and its surrounding mountains, whereas the validation of the results from other areas is mostly based on the literature (e.g., [45,46,49]).

### *3.2. Extraction of Basic Geomorphometric Parameters*

Based on a digital elevation model derived from TanDEM-X data (12-m horizontal resolution; please note that the elevations received from the TanDEM-X are ellipsoidal heights; the undulation of the geoid is around 40 m at the coast [23,24]), selected geomorphometric analyses [84] were conducted using various modules implemented in GRASS GIS [85] and SAGA GIS [86] in QGIS 3.8 [82]. Computed geomorphometric derivates were shaded relief, slope, geomorphons, aspect, topographic position index and topographic wetness index (Table 1). Zonal statistical analyses of geomorphological subunits were processed using the *Zonal statistics* module in QGIS 3.8 [82].

**Table 1.** Geomorphometric derivates (based on TanDEM-X data [23,24]) used for the identification of landforms in this study.

| Derivate | Module | Interpretation |
|---|---|---|
| Shaded relief | *Hillshade* | Shaded relief representation of the terrain surface. |
| Slope | *r.slope.aspect* [87] | The slope angle of a raster pixel. |
| Geomorphons | *r.geomorphon* * [88] | A recognition approach for the classification and mapping of the ten most common landform elements. |
| Aspect | *r.slope.aspect* [87] | The slope orientation of a raster pixel. |
| Topographic Position Index | *topographic position index (TPI)* [89,90] | Comparison of each raster pixel's elevation to the mean elevation of a specified neighborhood around that pixel. |
| Topographic Wetness Index | *r.topidx* [91–93] | The capacity of a raster pixel to accumulate water. |

* Regarding the parameters of *r.geomorphon* in this study, the outer search radius was set to be 1000 m, the inner search radius 50 m, and the flatness threshold 3 degrees. Geomorphon classes in the main text are shown in italics. Settings for other derivates remained at default values.

To obtain information on the major channel courses, river longitudinal profiles [94] (pp. 294–312) were extracted for several major river courses from the TanDEM-X data [69–72]. Noise in the river longitudinal profiles caused by reservoirs was manually excluded. Knickpoints were identified manually as inflexion points of the river longitudinal profiles.

To assess the shape of a mountain front, the mountain-front sinuosity index ($Smf = Lmf/Ls$; where $Lmf$ is the planimetric length of a mountain front along the footslope which is at the topographic break in slope, and $Ls$ is the length of a straight line at the former mountain front) was applied and calculated in QGIS 3.8 [82]. This represents the straight mountain front produced by active tectonics when the $Smf$ value is low, and sinuous or eroded front due to erosive processes and less active tectonics when the $Smf$ value is high [95,96].

Two swath profiles (Figure 1A: profiles A–A' and B–B'), i.e., the mean, maximum, and minimum elevation of equally spaced rectangles (here 500 × 6000 m) along the profile line (midline) [97], were calculated using GRASS GIS modules (v.mkgrid, v.rast.stats, and v.to.points) via QGIS 3.8 to determine topographic differences.

## 4. Results

### *4.1. General Geomorphological Characteristics*

The relief of the Bakırçay and Madra River catchments and their adjacent coastal areas can be grouped into three major landform types: (1) upland landforms including ridge, slope with debris cover and with bare rock, and valley with or without fluvial infill; (2) lowland landforms; and (3) anthropogenic landforms (Figure 4).

In the mountainous areas, upland landforms prevail, of which ridges and slopes with debris cover dominate. Outcropping bare rocks occur locally. Most of the perennial and intermittent river valleys are filled with fluvial deposits, whereas their tributary valleys in general have distinctly steeper inclining stream beds than the receiving streams and lack fluvial infills. Furthermore, anthropogenic landforms, including reservoirs, mines, and agricultural terraces, are widespread in the mountainous area. Alluvial landforms refer to the plains aggraded by the Bakırçay River; paleochannels in the lower Bakırçay plain document the anastomosing character of the Bakırçay River before straightening and embanking. To drain the lower Bakırçay plain, a wide network of canals was installed. The coastal areas are characterized by littoral plains and the deltas of Bakırçay and Madra Rivers. In the transition to the plain areas, the footslopes are fringed by colluvial deposits, locally interfingering with fan deposits from mountain rivers.

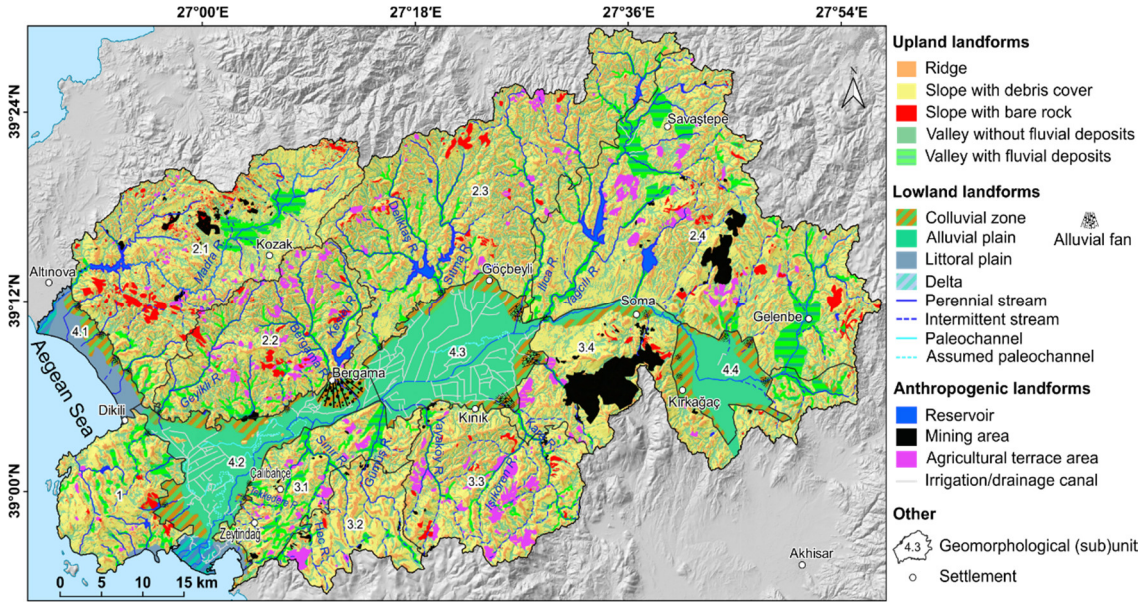


**Figure 4.** Geomorphological map of the Bakırçay and Madra River catchments according to the classification rules in Table S1 [83]. Note that paleochannels and terraces are not exhaustive. Geomorphological (sub)units are indicated by numbers; for territorial extent of the geomorphological (sub)units see Figure 1C.

The entire area of the Bakırçay and Madra River catchments has a mean elevation of ca. 377 m (σ = 233 m) with an elevation range of ca. 1432 m (Table 2). Corresponding to the mountainous relief, the slope inclination averages around 12°, with steep slopes regularly exceeding 10° in the mountains and flat–gentle terrain less than 3° in the plain areas (Table 2; Figure 5A). Landform units as displayed by geomorphons are dominated by *slopes* and *spurs* in the mountainous areas whereas the geomorphon *flat* prevails in plain areas (Figure 5B). All of these geomorphometric parameters clearly show spatial diversities in different (sub)units (Figure 5 and Figure S7).

**Table 2.** Geomorphological parameters in the four geomorphological units and their subunits of the study area (see Figure 1C for the (sub)units).

| Geomorphological (Sub)Units | | Area (km²) (Percentage) | Mean Elevation * (m) (Elevation Range (m)) | Slope (°) (σ) | TWI (σ) |
|---|---|---|---|---|---|
| **Total area** | | 4124 (100%) | 377 (1432) | 11.6 (9) | 6.4 (1.7) |
| Kara Dağı Mountains | **1** | **198 (5%)** | **221 (860)** | **11.3 (8)** | **6.7 (1.7)** |
| | **2** | **2320 (56%)** | **452 (1387)** | **13.7 (9)** | **6.1 (1.7)** |
| | 2.1 | 516 (13%) | 529 (1337) | 13.7 (8) | 5.9 (1.7) |
| | 2.2 | 332 (8%) | 437 (1110) | 18.3 (9) | 5.8 (1.7) |
| | 2.3 | 644 (16%) | 436 (1171) | 14.8 (8) | 6.1 (1.6) |
| | 2.4 | 829 (20%) | 423 (880) | 10.9 (8) | 6.5 (1.7) |
| Yunt Dağı Mountains | **3** | **988 (24%)** | **411 (1249)** | **12.9 (9)** | **6.4 (1.7)** |
| | 3.1 | 179 (4%) | 187 (423) | 9.6 (6) | 6.6 (1.7) |
| | 3.2 | 145 (4%) | 516 (1038) | 11.1 (7) | 6.2 (1.6) |
| | 3.3 | 310 (8%) | 427 (1152) | 15.5 (8) | 6.4 (1.8) |
| | 3.4 | 354 (9%) | 423 (742) | 12.9 (10) | 6.9 (1.5) |
| | **4** | **618 (15%)** | **92 (349)** | **1.9 (3)** | **6.9 (1.8)** |
| | 4.1 | 64 (2%) | 53 (183) | 2.1 (3) | 6.9 (1.8) |
| | 4.2 | 219 (5%) | 55 (229) | 2.2 (3) | 6.9 (1.8) |
| | 4.3 | 240 (6%) | 88 (182) | 1.4 (4) | 6.9 (1.7) |
| | 4.4 | 94 (2%) | 213 (133) | 1.7 (2) | 7.0 (1.8) |

* Elevation: ellipsoidal height, based on TanDEM-X data [23,24].

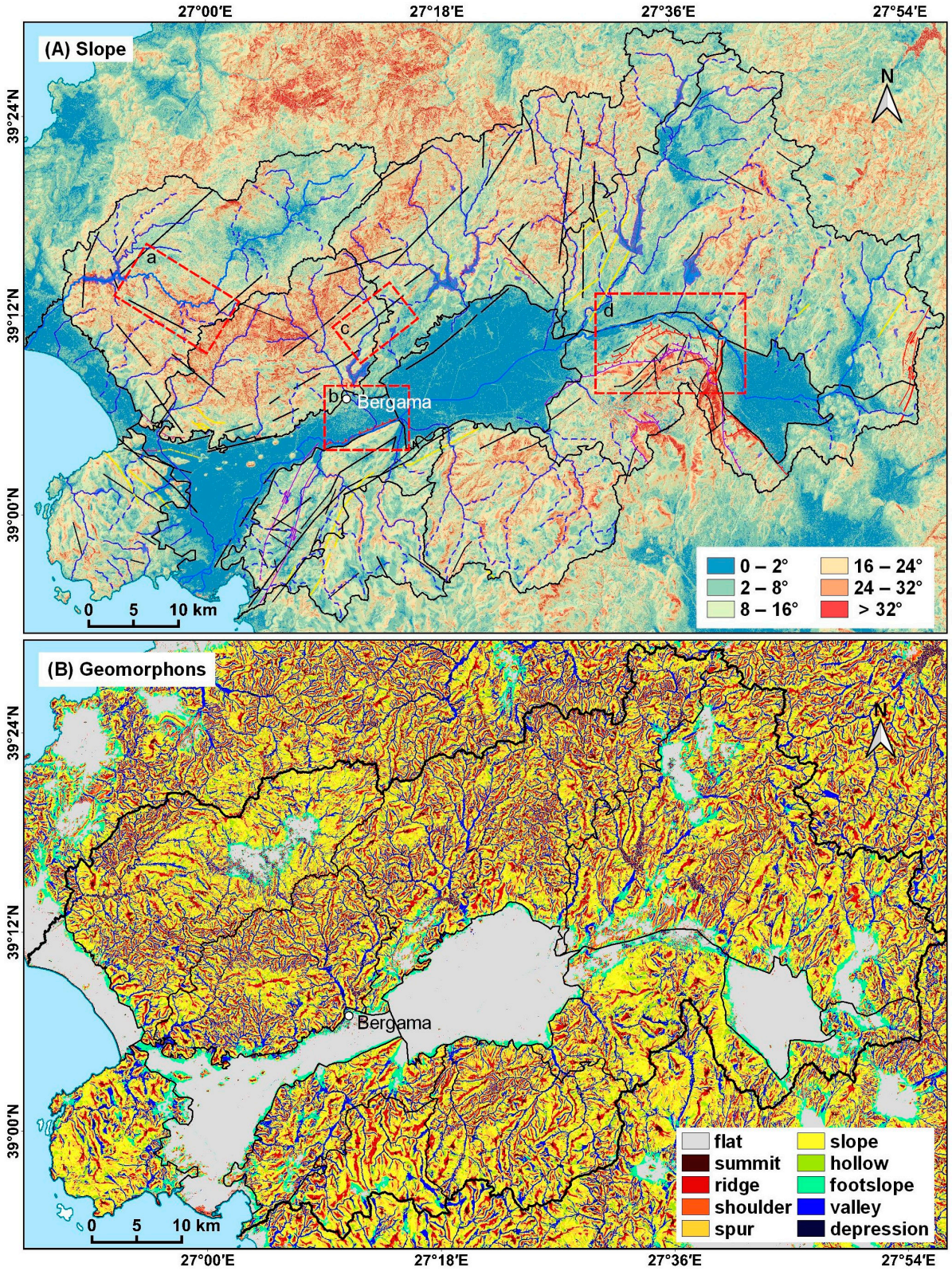


**Figure 5.** Morphometric characters of the Bakırçay and Madra River catchments. (**A**) Slope with perennial streams (streams were based on [69–72]) and faults (for fault legends see Figure 2; the red dashed rectangles numbered with a, b, c and d denote the geomorphological features under the impacts of tectonics, see the Discussion section). (**B**) Geomorphons. See Figure 1C for the geomorphological (sub)units.

Our results show extensive asymmetrical features of the Bakırçay and Madra River catchments, as evident in their geomorphometric characteristics. In particular, the asymmetry between the Northern Highlands and the Yunt Dağı Mountains surrounding the (western and eastern) lower Bakırçay plain is pronounced (Figure 6). The swath profile characterizes the asymmetry between the mountains surrounding the western lower Bakırçay plain (Figure 6: profile A–A′), viz., the Kozak Mountains to the north, and the western Yunt Dağı Mountains to the south. The eastern lower Bakırçay plain, with the Northern Highlands adjoining to the north and the eastern Yunt Dağı Mountains adjoining to the south (Figure 6: profile B–B′), is also asymmetrical, although with less-distinct geomorphological features.

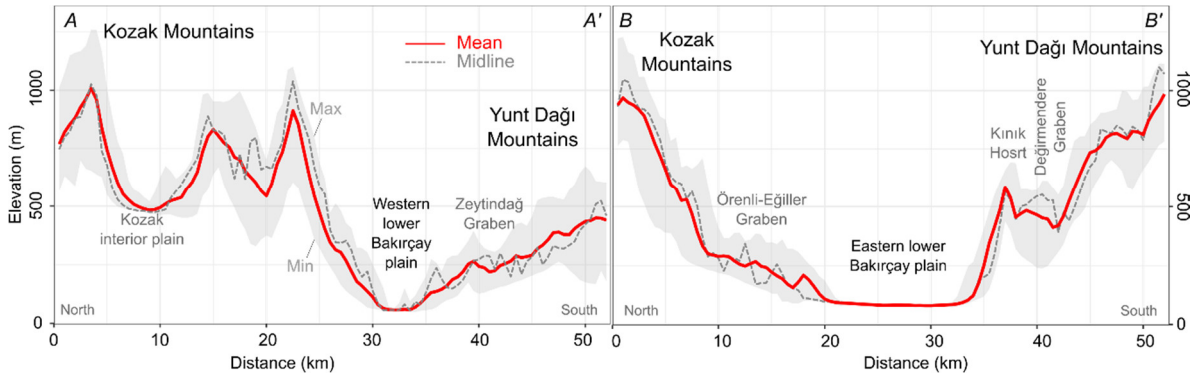


**Figure 6.** Swath profiles (for location see Figure 1A), indicating distinctly asymmetrical geomorphological characteristics between the Northern Highlands and Yunt Dağı Mountains surrounding the western lower Bakırçay plain (A–A′) and the eastern lower Bakırçay plain (B–B′). Note: 20× vertical exaggeration.

### *4.2. Major Geomorphological Units*

Corresponding to the major lithological (Figure 2) and geomorphological characteristics (Figure 4), the study area was divided into the four major geomorphological units—1—Kara Dağı Mountains, 2—Northern Highlands, 3—Yunt Dağı Mountains, and 4—Plain areas—with a total of thirteen subunits (Figure 1C).

#### 4.2.1. Geomorphological Unit 1—Kara Dağı Mountains

Geomorphological unit 1 corresponds to the Kara Dağı Mountains and covers an area of 198 km$^2$ (~5% of the study area; Table 2); this unit is not further subdivided. The Kara Dağı Mountains are dome-shaped, with the highest elevation at its central southwestern part (ca. 860 m a.s.l.) and circumferentially gently decreasing slopes (Figure 1A). In its eastern part, slopes generally incline less than 16°, whereas in its western part slopes reach inclinations up to 30° (Figure 5A). In its eastern part, narrow elongated *valleys* less than 1 km wide cut through a rolling landscape of *slopes* and *ridges*; extended *slope* areas occur at the western part of the Kara Dağı Mountains at its dip to the Aegean (Figure 5B). Agricultural terraces occur locally along the elongated valley flanks; these valleys are mostly infilled with shallow fluvial and colluvial deposits (Figure 4). Bare rocks are dominantly exposed at the southeastern upslope areas, whereas the downslope connecting footslope is covered by colluvial deposits, interfingering with littoral deposits of the Bay of Elaia (Figure 4).

#### 4.2.2. Geomorphological Unit 2—Northern Highlands

Geomorphological unit 2 corresponds to the Northern Highlands, which include the major Kozak Mountains (subunits 2.1 and 2.2), Korucu Dağları Mountains (subunit 2.3), Golcük Dağları Mountains (subunit 2.4), and their intramountainous basins (Figure 1A). This is the largest geomorphological unit in the study area, covering more than half of its area (Table 2). Subunits 2.1–2.3 were separated based on the major drainage divides, whereas subunit 2.4 was delineated according to differences in parent rocks with sed-

imentary rocks characterizing subunit 2.4, and mainly volcanic and pyroclastic rocks characterizing subunit 2.3. The Madra River (subunit 2.1) directly flows through the Altınova–Dikili littoral plain into the Aegean Sea.

**Geomorphological subunits 2.1 and 2.2** correspond to the Kozak Mountains, with the Madra River catchment draining the northern part of the Kozak mountains delineated as subunit 2.1. The Kozak Mountains have a mean elevation of around 530 m a.s.l. in subunit 2.1 and 440 m a.s.l. in subunit 2.2, with a total elevation range c. 1400 m (Table 2). Slope inclinations average 18° (Table 2) and locally reach a maximum of 80° (Figure 5A). Within the Kozak Mountains, the Kozak interior plain at 500–600 m a.s.l. altitude is located as a NE-striking intramountainous basin. The basin floor is filled by sediments, with the fluvial deposits of the Madra River forming overlying strata (Figure 4) [51]. The relief of the Kozak interior plain is shallow (<3°), corresponding to its high topographic wetness index (TWI) values (Figure S7C). The predominating geomorphons are *ridges*, *spurs*, *slopes*, *hollows*, and *valleys* in the mountainous areas beyond the Kozak interior plain (Figures 5B and 7). The high heterogeneity of the relief is also displayed by small scale changes in the values of the topographic position index (TPI) (Figure S7B).

Headwater areas of the Madra, Geyikli, Bergama, and Kestel Rivers rise from the Kozak mountains (Figure 4). Due to year-round spring discharge, these rivers sourcing from the Kozak Mountains are perennial. The river courses of the Madra River and the Kestel River show clear rectangular drainage patterns [43,51] (Figure 5A: a). The Madra River is dammed midstream at the transition of the Kozak Mountains into the coastal plain (Figure 4). Valley slopes are only rarely terraced, with agricultural terraces predominantly occurring at the Kozak Mountains' southern slopes (subunit 2.2) (Figure 4). Tributaries sourcing from the Kozak Mountains are short and intermittent, with valley infills predominantly found along their lower courses (Figure 4). Longitudinal profiles of the river courses (subunit 2.2) have a distinct concavity with steep upstream channel gradients that rapidly decrease at the mountain's foot zone and achieve a stretched characteristic in the downstream part (Figure 8), whereas flowing through the Kozak Mountains, repeatedly occurring knickpoints mark riffles and rapids (Figure 8).

Along the southwestern ridges of the Kozak Mountains, extended areas with outcropping bedrock occur (Figure 4). These locations frequently coincide with small extraction areas and small stone quarries, spread particularly across the northern slopes of the Kozak interior plain (subunit 2.1). Due to the plutonic rocks forming the northern and western part of the Kozak mountains, outcropping bedrock corresponds to granite boulders and their weathering products (Figure S4A). The Ovacik Gold Mine [21,98] is located at the southern footslopes of the Kozak Mountains at the transition to the western lower Bakırçay plain (Figure 2).

**Geomorphological subunits 2.3 and 2.4** exhibit a NE-striking depression–mountain–depression pattern, including the major morphotectonic landforms (from west to east): the Örenli–Eğiller Graben, Korucu Dağları Mountains, Savaştepe interior plain, Gölcük Dağları Mountains, and Gelenbe interior plain (Figures 1A and 2). The Örenli–Eğiller Graben (100–300 m a.s.l.) is characterized by a slightly rolling landscape with an average inclination of <6° and an average TWI of seven; the graben floor is covered by fluvial and colluvial deposits with locally occurring landslides. Graben flanks, and the Kozak Mountains to the northwest and the Korucu Dağları Mountains to the east, have a strong relief, with c. 15° average inclination (subunit 2.3; Figure 5A). The basin structures of the Savaştepe interior plain and the Gelenbe interior plain are located at an elevation of c. 250 m a.s.l.; like the Kozak interior plain, they are filled with fluvial and colluvial deposits, resulting in a shallow relief with an average TWI of 7.1 (Figure S7C). Outcropping bare rocks are widely scattered across the mountainous areas of subunits 2.3 and 2.4 (Figure 4).

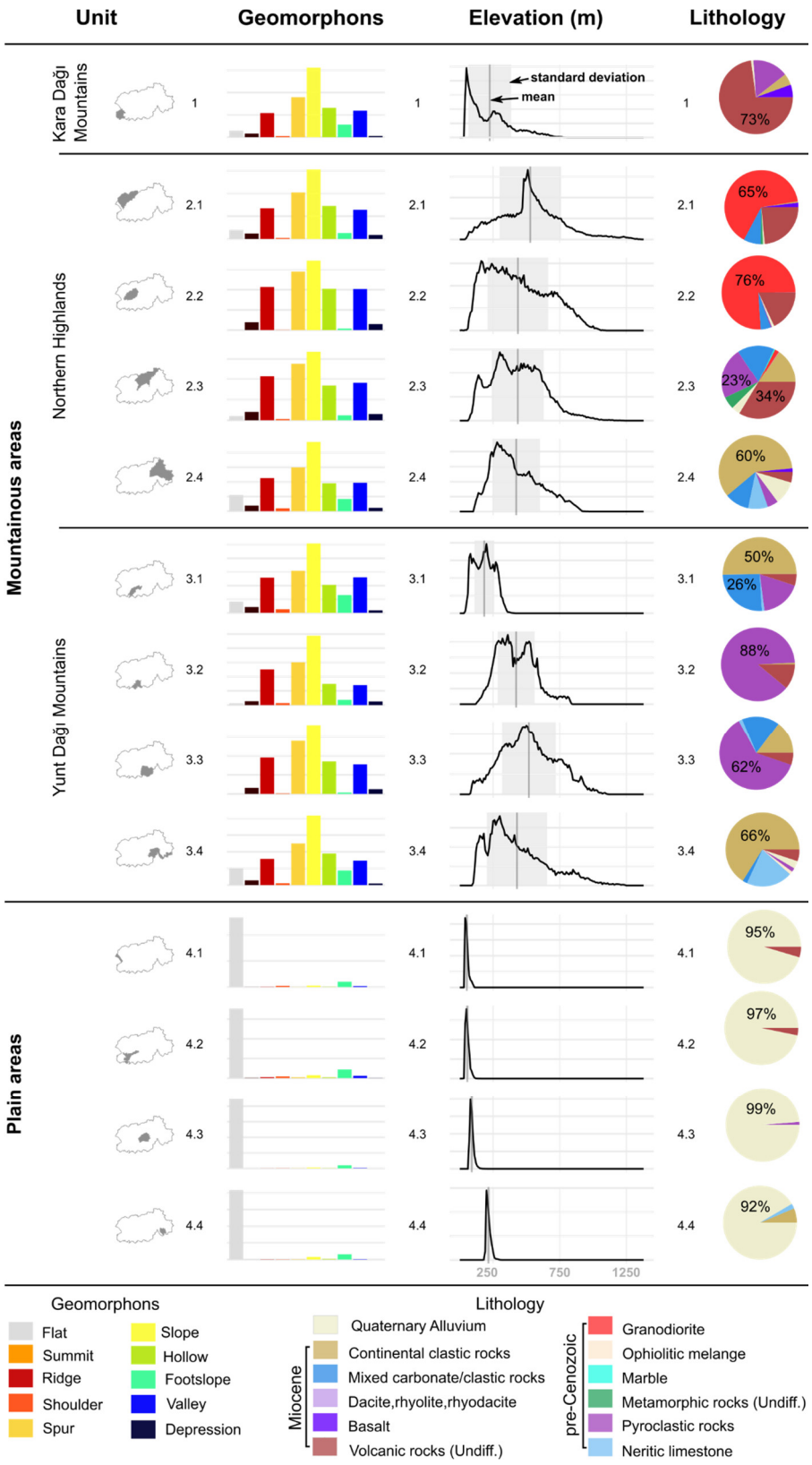


**Figure 7.** Distribution of the morphometric and lithologic characteristics of the Bakırçay and Madra River catchments, outlining geomorphological subunit distribution of geomorphons and elevation; y-axis shows the total number of pixels per geomorphon and per altitude range. Pie charts show the distribution of lithology.

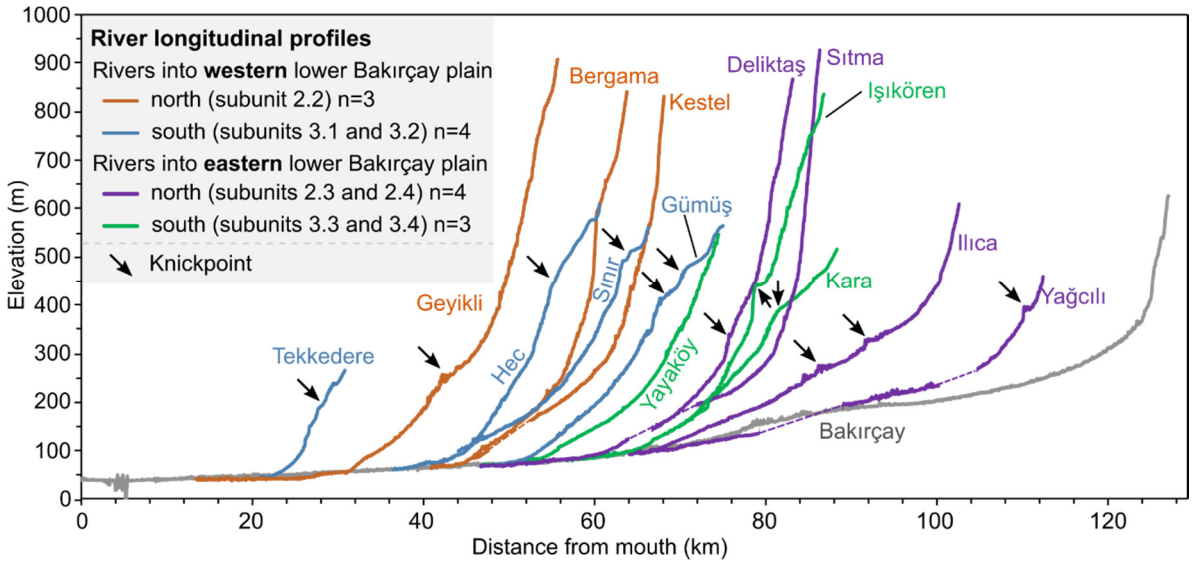


**Figure 8.** Longitudinal profiles of channel courses and major knickpoints in the Northern Highlands (geomorphological subunits 2.2–2.4) and Yunt Dağı Mountains (geomorphological subunits 3.1–3.4) enclosing the lower Bakırçay plain (see Figure 4 for the river courses). Note: c. 50× vertical exaggeration; reservoirs were manually modified with dashed lines.

Tributaries of Bakırçay River with sources in the Korucu Dağları Mountains (subunit 2.3) and the Gölcük Dağları Mountains (subunit 2.4) show concave longitudinal channel profiles, which are typical for mountainous tributaries with very steep upper courses repeatedly interrupted by knickpoints (Figure 8). A clear relationship between the degree of concavity and the ratio of the channel length to the altitude of the headwater area can be observed, indicating stronger morphodynamics for the Deliktas and Sitma Rivers than for the Ilica and Yağcılı Rivers.

Reservoirs have been built at the middle-lower reaches of the major streams (Deliktaş, Sıtma, and Yağcılı) (Figure 4), some of which collect runoff from drainage basin areas up to 450 km$^2$ in size, e.g., the Sevişler reservoir on the Yağcılı River between the Korucu Dağları and Gölcük Dağları Mountains [99] (Figure 4). A large mining area is located next to the Soma–Kolin Thermal Power Plant in the Korucu Dağları Mountains (subunit 2.4; Figures 2 and 4) covering an area of c. 15 km$^2$. Agricultural terraces mainly occur on the Gölcük Dağları Mountains (subunit 2.3; Figure 4).

#### 4.2.3. Geomorphological Unit 3—Yunt Dağı Mountains

Geomorphological unit 3 corresponds to the northern part of the Yunt Dağı Mountains and incorporates about one quarter of the research area (Table 2). Including the Maruflar Horst, the ridges along the divide reach elevations >1200 m a.s.l. (Table 2) and are widely composed of pyroclastic rocks (88% of its area). The Zeytindağ and Yayaköy grabens (subunit 3.1; Figure 2) confine the Maruflar Horst to the NW and N, both being infilled by Quaternary fluvial deposits (Figure 4). In the NE of Maruflar Horst, Değirmendere Graben and Kınık Horst (subunit 3.3) display the basin–range structure, building the transition into Bergama Graben. The Kınık Horst corresponds to a block of uplifted Miocene carbonates, whereas adjacent eastern Yunt Dağı Mountains (subunit 3.4) are mainly built out of continental clastic rocks (Figures 2 and 7).

**Geomorphological subunit 3.1.** The ground level of the Zeytindağ and Yayaköy grabens (subunit 3.1) is at 180–190 m a.s.l. altitude; Quaternary graben infills cause a moderate relief with inclinations <10° (Table 2 and Figure 5A). Streams are generally short and intermittent, especially those close to Çalıbahçe and Zeytindağ (Figure 4). Additionally, agricultural terraces and mining areas are widely spread throughout the area (Figure 4).

**Geomorphological subunit 3.2.** The Maruflar Horst (subunit 3.2) has a mean elevation of c. 516 m and forms the highest area of the Yunt Dağı Mountains. The horst is in the

headwater areas characterized by small *flats* and *footslopes* (areas of less than 2 km$^2$), and wide and elongated *ridges* and *slopes* being up to c. 3 km wide (Figure 5B). In the headwater areas, valleys are saucer-shaped and infilled by shallow fluvial deposits. Valleys are deeply incised and still under active incision at the confluence into the Zeytindağ and Yayaköy grabens. At the lower courses of the Sınır and Gümüş Rivers, in particular, the valley floors widen and are infilled by fan deposits; fans gently incline and cover areas of c. 2 km$^2$ (Sınır) and 5 km$^2$ (Gümüş) (Figure 4). Agricultural terraces occur predominantly on the uphill graben shoulders of Zeytindağ and Yayaköy grabens.

Channel courses in the western Yunt Dağı Mountains (subunits 3.1 and 3.2) show distinct convex shapes in their longitudinal profiles in the upstream areas, tracing the transition of saucer-shaped valleys in plateau-like environments of the headwater areas to the graben flanks (Figure 8). Repeatedly occurring knickpoints mark fault lines crossed by the river courses (see Gümüş, Tekkedere, and Sınır Rivers in Figure 8).

**Geomorphological subunit 3.3.** The basin–range structure of Kınık Horst and Değirmendere Graben (subunit 3.3) covers an elevation range of 1152 m; the 15.5° average slope inclination documents the strong relief (Table 2). Landform units are characterized by short and narrow *ridges*, *slopes*, and *valleys*, whereas there is a lack of *flats* (Figure 7); overall, the landscape of Kınık Horst and Değirmendere Graben is highly heterogeneous (Figure 5B). Corresponding to the strong relief, valleys are deeply incised, with fluvial deposits only occurring in basin-like valley openings, such as in the lower course of Yayaköy River (Figure 4). The size of most of these basins is less than 1 km$^2$. Slopes are widely covered by debris and only locally bare rocks crop out (Figure 4); correspondingly, agricultural terraces are widely distributed.

**Geomorphological subunit 3.4.** The eastern Yunt Dağı Mountains (subunit 3.4) are characterized by steep slopes of more than 30° inclination, particularly at the areas adjoining to the Soma valley and upper Bakırçay plain (Figure 5A). The slopes are widely covered by debris, whereas bare rocks only locally crop out. Soma valley, with its 1–2-km-wide valley floor, is also part of subunit 3.4, expressed by a distinct occurrence of *flats* (Figure 5B). Kısrakdere Coal Mine, with a quarrying area of more than 40 km$^2$, is located in the central eastern Yunt Dağı Mountains (Figure S4E). Agricultural terraces occur only rarely (Figure 4).

Longitudinal profiles of channel courses in the eastern Yunt Dağı Mountains (subunit 3.3 and part of subunit 3.4) have a concave shape, locally interrupted by convex knickpoints, e.g., Kara and Işıkören Rivers (Figure 8). In particular, the longitudinal channel profile of the Işıkören River is marked by strong inclinations at the upper and middle courses, and a distinct knickpoint in the middle course.

#### 4.2.4. Geomorphological Unit 4—Plains

The plain areas (geomorphological unit 4) are widely flat, with inclinations of less than 3° (Figure 5A). Fluvial, colluvial, and littoral Quaternary deposits cover the plain areas (Figure 4). Subunit 4.1 corresponds to the littoral area. Subunits 4.2–4.4 display the alluvial plains of the Bakırçay River, separated by the Bergama fan and Soma valley into the western lower Bakırçay plain (subunit 4.2), eastern lower Bakırçay plain (subunit 4.3), and upper Bakırçay plain (subunit 4.4). The width of the lower Bakırçay plain in its central part (around the Bergama fan) is 2–3 km, whereas it increases to c. 10 km in the western lower Bakırçay plain (subunit 4.2) and c. 13 km in the eastern lower Bakırçay plain (subunit 4.3).

The headwater areas of Bakırçay River are located in the Gölcük Dağları Mountains from where the river course heads southward until reaching the basin of the upper Bakırçay plain (subunit 4.3). In the upper Bakırçay plain, the river flows westward before turning north when reaching the eastern spur of the Yunt Dağı Mountains. In particular, the Bakırçay River close to Soma flows along a meandering valley, which is predetermined by the adjoining mountain ranges and the local fault systems.

Downstream of Soma, the valley opens to the lower Bakırçay plain. Bakırçay River flows in a WSW direction in the eastern lower Bakırçay plain (subunit 4.3) and turns to

the SW after passing the Bergama fan (western lower Bakırçay River plain; subunit 4.2). Throughout the lower Bakırçay plain, the Bakırçay River flows almost along the footslopes of the Yunt Dağı Mountains.

At the transition of the western lower Bakırçay plain into the Aegean Sea, the delta of the Bakırçay River, with an area of 14 km$^2$, is developed between the modern settlement of Çandarlı (subunit 1) and the Bay of Elaia, which is separated from the delta by the Bozyertepe ridge, a spur of the Yunt Dağı Mountains (subunit 3.1) [38].

**Geomorphological subunit 4.1.** The Altınova–Dikili littoral plain adjoins the footslopes of the western Kozak Mountains. Correspondingly, the area is composed of a 1–2-km-wide zone covered by coastal deposits interfingering with colluvial deposits along the western footslopes of the Kozak Mountains (Figure 4). Fluvial deposits from the Madra River aggrade and gradually form the Madra River delta downstream from the modern settlement of Altınova [43]. The littoral plain also connects to the western lower Bakırçay plain (subunit 4.2) through a narrow corridor close to Dikili.

**Geomorphological subunit 4.2.** At the northern transition zone between the Kozak Mountains and the western lower Bakırçay plain, colluvial deposits and alluvial fans cover the foot zone of the Kozak Mountains, reaching a width of 2 km (Table 3). In contrast, at the southern boundary of the western lower Bakırçay plain, the colluvium along the footslope of the Yunt Dağı Mountains has a maximum width of 500 m (Figure 4). In addition, the mountain-front sinuosity index (Smf) of the Kozak Mountains and the Yunt Dağı Mountains differs, with a distinctly lower value for the Yunt Dağı Mountains (2.16) than for the Kozak Mountain front (2.73) (Table 3). In the northern part of the Bergama Graben, small dome-shaped volcanic hills occur (Figure 2), e.g., the Kalarga Tepe and Eğrigöl Tepe.

**Table 3.** Mountain-front sinuosity index (Smf) and extension of colluvial deposits in the lower Bakırçay plain.

| Location | | Lmf (m) | Ls (m) | Smf | Extension of Colluvial Deposits (km) |
|---|---|---|---|---|---|
| Western lower Bakırçay plain | north | 76.29 | 27.97 | 2.73 | 0.5–2 |
| | south | 48.17 | 22.32 | 2.16 | <0.5 |
| Eastern lower Bakırçay plain | north | 53.83 | 20.11 | 2.68 | <0.5 (west part); 0.5–3 (east) |
| | south | 60.80 | 20.29 | 3.00 | |

The Bergama fan separates the western lower Bakırçay plain from the eastern lower Bakırçay plain. The city of Bergama was founded in the root-zone of the fan and provides its name. The Bergama fan covers an area of approximately 14 km$^2$ and receives sediments from the Kozak Mountains by means of the Bergama River and Kestel River, which have a combined drainage basin area of 156 km$^2$. Other fans deposited in the western lower Bakırçay plain mostly cover areas of 1–2 km$^2$ and are deposited by Bakırçay tributaries with drainage basin areas <120 km$^2$. In the western lower Bakırçay plain, widespread river regulation measures occur, including canals, stream straightening (e.g., the Doğramacı canal of the Geyikli River), and the construction of river embankments up to 5 m high [10]. Abandoned channels and cut-off meanders occur predominantly close to the straightened and embanked river courses (Figure 4). The extensive drainage of wide areas of the lower Bakırçay plain influences local runoff regimes and water budgets.

**Geomorphological subunit 4.3.** In the eastern lower Bakırçay plain (ca. 88 m; Table 2), colluvial deposits at the eastern transition zone from Göçbeyli to Kınık are up to 3 km wide, whereas in the western transition areas they are generally less than 0.5 km wide (Table 3). Alluvial fans with areas of 2–5 km$^2$ primarily occur in the east of the zone (Figure 4). The sinuosity value of the eastern Yunt Dağı Mountains' front (3.00) is slightly higher than that of the Northern Highlands (2.68) (Table 3).

**Geomorphological subunit 4.4.** The mean elevation of the upper Bakırçay plain (subunit 4.4) averages ca. 213 m (Table 2). The slopes to the Akhisar plain of the Gediz River catchment are gentle; thus, they can be easily connected [17,30]. At the footslopes along the upper Bakırçay plain, abundant colluvial sediments were deposited (Figure 4),

building a two-kilometer-wide transition zone at the east (from Soma to Kırkağaç) and decreasing in extent to the west. The alluvial fans of the Bakırçay River tributaries have areas of less than 1 km$^2$. Only a few canals are found in the upper Bakırçay plain.

## 5. Discussion

The distinct asymmetry of the topography in the Bakırçay and Madra River catchments (Figure 6) is an expression of the strong impact of tectonic movements. Locally varying rates of uplift and sinking due to tectonic compression and divergence resulted in a small-chambered relief with sharp borders between the different geomorphological units. These effects are amplified by the inclination of the rock strata forming the mountainous areas due to their locally highly variable characteristics of strike and dip. This diverse landscape promoted the area's suitability for usage since the Holocene.

### *5.1. Development of the Major Landform Units*

The **Kozak Mountains** (geomorphological subunits 2.1 and 2.2) are characterized by high average elevation and steep slopes (Figure 6: A–A'), a NW-trending large-scale bare rock association, and rectangular drainage courses. The mountains comprise Miocene volcanic centers characterized by andesitic volcanism, which surround the plutonic core of the Kozak interior plain [100]. In parallel, compressional forces from the westward drift of the Anatolian plate during the Miocene caused an uplift of the area [3,50]. During the Miocene, Pliocene, and early Quaternary, the uplift of the Kozak Horst and subsidence of surrounding grabens shaped the Kozak Mountains (Figure 2) [45,51,101]. The bare rock association dominating on the western ridges of the Kozak Mountains (subunit 2.1, Figure 4) is associated with the NW–SE-striking Altınova–Dikili fault zone [72] (Figure 2). Steep slopes are deeply fissured, resulting in a high infiltration capacity and shallow soils [74]. The rectangular flow pattern of the Madra River is controlled by the local fault system (Figure 5A) and the Mio-Pliocene lava flows [51]. In addition to lithological differences between pyroclastic and continental clastic rocks [60] (Figure 2), the rectangular drainage pattern of the Kestel River can also be attributed to the fault system [72] (Figure 5Ac).

A peculiarity of the Kozak Mountains is the wide and flat Kozak interior plain (geomorphological subunit 2.1), a large intramountainous basin filled by Quaternary sediments. Granodiorite boulders in the northern margin of the Kozak interior plain document spheroidal weathering (Figure S4A), building a typical granite landform [102]. In addition, the slopes formed in the granodioritic bedrock result in frequently outcropping bare rock covered by a thin layer of weathering products. Comparable interior plains as large sediment sinks can be found at Savaştepe and Gelenbe, in geomorphological subunit 2.4 [103]. The formation of the Savaştepe interior plain can be linked to the NE-trending İzmir–Ankara Suture Zone (Figure 2) [25,48].

Compared to the Yunt Dağı Mountains (see below), the colluvial and alluvial fan deposits at the footslopes of the Kozak Mountains are largely extended, being directly related to the size and relief of the drainage basin, which indicate high erosion dynamics [94,104–106]. The upper parts of the Geyikli, Bergama, and Kestel Rivers' longitudinal profiles, which each have headwater areas located in the Kozak Mountains (Figure 8), clearly indicate high relief, resulting in strong incision processes [107,108]. The knickpoints along the longitudinal profiles are indicative of faults if the bedrock remains unchanged [94,109].

In the western **Yunt Dağı Mountains**' hinterland, the Maruflar Horst (subunit 3.2) developed in a manner geologically similar to the Kozak Horst [45]; the bedrock of the Maruflar Horst is dominated by pyroclastic rocks formed by Early to Middle Miocene volcanism [45,60].

The **Zeytindağ and Yayaköy grabens** (subunit 3.1) form local sedimentary sinks. The NE-trending Zeytindağ Graben to the south of the Bakırçay plain—together with Örenli–Eğiller Graben to the north—developed under the Late Miocene east–west extension between the Kozak Horst and the Göçbeyli Horst [45]. The formation of the orthogonal Bergama Graben during the Pliocene separated the Zeytindağ–Örenli–Eğiller Graben into

two units [45], both having the typical topographical characteristics of graben structures with flat infilled graben floors and step faults along the graben shoulders [110] (p. 74). The straight mountain fronts of the Yunt Dağı Mountains display regional tectonics, particularly the Holocene normal faults, e.g., the Sindel normal fault [70] (Figure 5Ab).

In comparison to the Kozak Mountains, the gentler relief in the western Yunt Dağı Mountains is expressed in less-pronounced channel gradients [111] (Figure 8). The convex-upward shape of the Bakırçay tributaries draining the Yunt Dağı Mountains indicates the plateau-like relief in the headwater area, whereas the repeatedly superimposed concavities in their longitudinal profiles show their high rate of incision with rapid adjustment close to the Bakırçay plain [109]. Fluvial sediments can only be found along the river courses in local sinks wherever there is a break in inclination corresponding to the system of sediment cascades [52–54]. Overall, the Bakırçay tributaries flowing from the Yunt Dağı Mountains show an immature stage of channel development [94], with frequently occurring knickpoints, indicating Quaternary faults [69,72] (Figure 2). Although perennial streams such as the Sınır and Gümüş Rivers merge into the Bakırçay plain, the alluvial fans are only very slightly convex-shaped, due to the shallow inclination of the tributaries' river courses and the corresponding shallow relief of their drainage basins [18].

In the north of the eastern Lower Bakırçay Plain, the NE-trending **Örenli–Eğiller Graben** (Figure 2) exhibits a similar elevation distribution and gentle slopes to those of the Zeytindağ Graben (subunit 3.1) [45]. The basis of the Örenli–Eğiller Graben forms a sink, preventing most of the sediment eroded from the mountains from reaching the eastern lower Bakırçay plain (Figure 4). The steep channels of the upper Deliktaş and Sıtma Rivers indicate the lasting uplift of the Kozak Horst [94] (p. 306). The llıca and Yağcılı Rivers show less steep longitudinal channel profiles than the Deliktaş and Sıtma Rivers, indicating lower uplift rates in their headwater areas than at the Kozak Horst [94]. Knickpoints along llıca and Yağcılı River course profiles imply fault lines of the İzmir–Ankara Suture Zone [25]. Due to the large drainage basins of the llıca, Yağcılı, Deliktaş, and Sıtma Rivers, extended alluvial fans formed at their confluence into the eastern lower Bakırçay plain (Figure 4).

The **Kınık Horst** (subunit 3.3) in the south surmounts the eastern lower Bakırçay plain by approximately 500 m and steep slopes characterize its transition to the eastern lower Bakırçay plain (Figure 6: profile B–B'). Its sinuous mountain front (Smf = 3; Table 3) indicates low to moderate tectonic activities [112]. Only a narrow verge at the footslope of the Kınık Horst is covered by colluvial deposits (Figure 4). The two alluvial fans of the Yayaköy and Kara Rivers occur because their drainage basin sizes are distinctly larger than those deposited at the footslopes of the western Yunt Dağı Mountains. The rivers deeply incised into Kınık Horst; the lack of intermediate sediment storage areas resulted in large fan areas being slightly disproportionate to the size of their drainage basins.

**The Kara Dağı Mountains** to the west of the lower Bakırçay plain have a Miocene volcanic center [100] and form as the Kane peninsula reaching into the Aegean Sea. The N–S trending valleys and ridges in the Kara Dağı Mountains (Figure 4) correspond to Cenozoic NNW–SSE striking faults [49,69,71,73] (Figure 2). Extensive colluvial deposits in the southeast of the Kara Dağı Mountains in the transition zone to the western lower Bakırçay plain are indicative of high erosion activity, resulting in deeply incised valleys following faults [49].

The **lower Bakırçay plain** develops in the east–west trending Bergama Graben. Alluvial deposits of the Bakırçay River, in addition to colluvial and alluvial fan deposits from the adjoining mountains, are continuously aggrading the lower Bakırçay plain. Separating the upper and lower Bakırçay plain, the Soma valley, with a long and narrow shape, is controlled by a series of high-angle oblique-slip normal faults, active since the Pleistocene, with small lateral components that strike NE–SW, NW–E, N–S, and E–W [46,48,70] (Figure 2). The western extension of N-trending faults [70] between Soma and Kırkağaç forms a linear structure of steep slopes facing west.

The formation of the Bergama Graben started from the Early Pliocene [45,48]. During the Quaternary, two NNE- to NE-trending dextral oblique-slip fault segments at Zeytindağ–

Bergama and Kınık–Turgutalp deformed the former Bergama Graben into a transtensional pull-apart basin striking NE–SW with sediments up to 120 m thick [48]. Due to the influence of the former fault zone, the Zeytindağ Graben and the surrounding ridges (subunit 3.1) were moved to the NE (towards the city of Bergama), causing the constriction between the eastern and western lower Bakırçay plain [45,48]. Here, the straight channel pattern of the Bakırçay River (Figure 5A: b) displays the tectonic influence on the river course. Presumably due to the continuous uplift of the Kozak Mountains, the Bakırçay River flows close to the footslopes of the Yunt Dağı Mountains, contributing to the asymmetry of the plain [45].

An exceptional landform in the Plain Areas is the **Bergama alluvial fan**, which is formed from deposits of the Kestel and Bergama Rivers in the Northern Highlands. Mountainous relief [105] and seasonally high discharges allow high transport rates for the bedload deposited at the longitudinal gradient change at the transition from the Kozak Mountains to the Bakırçay Plain [105].

Widespread **paleochannels** in the lower Bakırçay plain indicate the formerly anastomosing channel pattern of the Bakırçay River, with strong deposition and redeposition dynamics during seasonal flood flows at least since ancient history [10,11]. During the Early–Middle Holocene, the Bakırçay floodplain was assumed to be narrower than today [11].

The most prominent **coastal landforms** in the study area are the Altınova–Dikili littoral plain and the deltas of the Madra and Bakırçay Rivers. The littoral plain is part of the NW-trending Ayvalik–Lesvos Graben, which subsided during the Quaternary [101] (p. 19). Similar to the southern Kozak Mountains, the tectonic movement caused steep slopes, which today merge into the coastal plain by colluvium deposited at the footslope [1,51]. The Altınova–Dikili coastal area is dominated by Pliocene–Pleistocene alluvial fans based on torrential deposits that extend into the Aegean Sea [2,101]. These coarse-detrital fan deposits were flooded by the Holocene marine transgression after 7000–6000 BP [101] and were subsequently overlain by alluvial delta deposits of the Madra River and the Karakoç River (the latter is located c. 5 km north to the Madra River) [39].

The corridor between the Altınova–Dikili littoral plain and the Bakırçay plain can be linked to the active tectonic activities at the Altınova–Dikili fault zone (Figure 2: ①) [113]. Tectonic activities along the fault zone are also responsible for the thermal springs occurring in this area, e.g., the Kaynarca thermal spring that emerged after the 1939 earthquake [113]. In addition to these effects of tectonics, the development of coastal areas was highly impacted by regional sea-level changes [1,114,115] and caused the deposition of interbedded coastal swamp–sandy marine sediments and terrestrial alluvial–deltaic deposits [38,43].

### *5.2. Usage Suitability and Human Impact during the Late Holocene*

Prehistoric and ancient settlements in the Pergamon Micro-Region are dominantly found in the flat–gently-inclining transition areas between the mountains and plains (Figure 1A) [12,18]. Those areas are easily accessible to diverse resources (including water, food, and building materials) and have geographical strategic significances (such as being flood-safe and providing through-traffic). Fertile plain areas provide the largest portion of the food supply of the micro-region [28]. Throughout **the Bakırçay plain**, settlements prefer flood-safe places, such as the piedmonts along the footslopes of the adjoining mountain areas [10]. In the western lower Bakırçay plain, some archaeological sites also occur close to the elevated volcanic cones, e.g., the Yeni Yeldeğirmentepe site (Figure 1A) [11]. The slightly rolling and flood-safe piedmonts at the footslopes of the mountains are currently the preferred locations for pathway and road networks [17]. Low-angle colluvial deposits attracted colonization and the foundation of cities, e.g., the modern cities of Soma (ancient Germe), Kırkağaç, and Kınık (Figure 1A) [17]. However, the flood-safe areas are not always "safe". Fluvial aggradation during Holocene transgression may occasionally flood the ancient human occupations [10], agricultural fields, and roads, which may hinder the continuous usage of plain areas.

The strong relief of the **Kozak Mountains** is widely unsuitable for settlements, and only the gently inclined colluvial deposits adjoining the Bakırçay plain are favored for agriculture [8,9]. An exception is the hill-top settlement of Kale Ağılı (ancient polis Atarneus) in the lower Geyikli drainage basin (Figure 1A), which benefited from its prominent topographical location and advantages such as a strategic position in terms of visual control, easy access to timber from a mountainous hinterland, and fertile agricultural land in the environs [9]. The foot-zone of the Kozak Mountains is a preferred area for the through-traffic between the coast and Bergama, i.e., between the ancient polis of Atarneus and Pergamon (Figure 1A) [17]. In addition, the flat relief and fertile fluvial sediments on the Kozak interior plain provide ideal conditions for agriculture (Figure S6). During antiquity, human settlements were found in the area, e.g., Perperene and Kytonion (Figure 1A) [17]. Similarly, the low inclinations and infilled unconsolidated sediments make the Örenli–Eğiller Graben suitable for agriculture (Figure S6) and settlements (Figure 1A) [17]. The Kozak Mountains have been incised by large rivers (the Madra and Bergama Rivers) that are integral parts of the road network, with connections among the Kozak interior plain (further to Adramytteion), the coastal areas, and ancient Pergamon (Figure 1A) already existing in ancient times [17]. In addition, the llıca, Yağcılı, Deliktaş, and Sıtma Rivers in the Northern Highlands formed deeply incised valleys that provided natural pathways connecting Pergamon with ancient settlements to the northeast and east, such as Ergasteria and Hadrianoutherai (Figure 1A) [17].

The **Bergama fan** is a terrestrial landform of high morphodynamics, characterized by frequent sheet-flow and rapid stream-channel shifts, which hampered settlement activities. However, after the incision of the Bergama River into its own deposits, the channel course stabilized, and the flooding risk was reduced. Consequently, natural advantages, including access to water (surface water and groundwater) for drinking and farming, fertile soils for food, and spaces for living, have attracted humans to settle in this area [105,116]. Some scholars regard the major reasons for the founding of ancient Pergamon adjacent to the Bergama fan were the fan's physiographic endowment, good accessibility of natural resources, and good strategic location [30,117,118]. In spite of the possible accessibility of water from the Bergama alluvial fan, gigantic aqueducts in ancient Pergamon were constructed for continuous water supply as a basic feature of civilized life during Hellenistic–Roman times, such as the aqueduct from the Kozak Mountains to the Acropolis of Pergamon (Figure 1A) built by Eumenes II (197–159 BC). This construction benefited not only from political, economic, and technical developments [20,58], but also from the geographical advantage of having the water source area in the topographically high Kozak Mountains.

For the Pergamon Micro-Region, most recent archaeological surveys in the gentle areas of the **Yunt Dağı Mountains** assume a large potential for human occupation [12,18,44,110]. Olive cultivation in the western Zeytindağ Graben has been reported since at least ~2.8 ka BP [40]. The local sediment sinks in the Yunt Dağı Mountains, including the fertile intramountainous basins and flat basin-like extended valleys at the river outlets, favor the development of small-scale settlements and agriculture, e.g., in the Tekkedere, Çalıbahçe, and Gümüş valleys (Figure 1A), in different archaeological periods at least since the Late Chalcolithic period [12,18,32,44,110]. In the Yunt Dağı Mountains, small *flats* with infilled saucer-shaped valleys served for the founding of small hamlets. The soils formed on the fluvial deposits of the saucer-shaped valleys attracted farming; the hamlets were also able to be used as rest areas for travelers on the route from Pergamon to southern cities such as Apollonis and Magnesia (Figure 1A) [17], proving the importance of the areas adjoining the plain for traffic purposes. However, due to the active tectonics, such as earthquakes and the resulting landslides, the settlements in the west Yunt Dağı Mountains may be abandoned and relocated occasionally [110].

The **Kara Dağı Mountains** make the Bakırçay valley unique along the Anatolian Aegean coast because they restrict the connection between the Bakırçay plain and the Aegean Sea to two narrow corridors [119] (p. 15). Settlement areas in the Kara Dağı

Mountains predominantly occur along the coastal zone and close to small rivers [17,27,44]. The fertile delta plains of Bakırçay and Madra Rivers favor agricultural activities [43], and their marshy ground also makes them widely unsuitable as settlement areas and for through-traffic. The site of the Hellenistic–Roman harbor city of Elaia [35,38] was chosen due to its protected location in the lee of the Kara Dağı Mountains. However, the shallow area of the Bay of Elaia was already silted during Roman times due to the high sediment load of the Bakırçay River and the adjacent slopes [38].

Currently, human activities in the Bakırçay and Madra River catchments and their adjacent coastal areas are not only affected by the characteristics of the natural environments, but also directly shape landforms and locally dominate the landscape.

Hydrologic constructions for water storage are common in the Northern Highlands. These constructions have affected discharge and resulted in reduced sediment transport and alluviation within the lower Bakırçay plain and coastal areas since the 20th century [1,8,10]. Mechanized, industrial-scale agriculture is conducted throughout the entire eastern and western lower Bakırçay plain due to (a) river regulation and straightening, (b) drainage by a network of ditches, and (c) flood protection resulting from the construction of dams along the course of the Bakırçay River [18].

Rich mineral resources such as coal [46,120,121] and gold [21,122] are widely extracted [98,123,124], resulting in the formation of mining areas of varying sizes throughout the study area. Coal mining areas are located in the eastern part of the area (Figure 2), i.e., the Soma coal basin, which is one of the largest economic lignite-bearing alluvial basins in Turkey, with lignite and kerogen as the main products [46,124]. A gold and silver mine is located at Ovacık–Narlica in the south of the Kozak Mountains (Figure 1A), where the precious metals formed during the Early Miocene [21,98]. Mining activities in this area started around 600 BCE under the rule of King Croesus and were further exploited during the Roman period (c. 400 CE) [21]. The modern Ovacik Gold Mine has been active since ca. 1990. Stone or sand quarries are widely distributed throughout the study area and are mostly small in size. The stone quarry at Asağı Çuma (Figure 1A) has been used at least since the Hellenistic period [22,123]. Mining of perlite, a weathering product emerging from the hydration of obsidian, is conducted in the western Yunt Dağı Mountains [18].

Agricultural terraces implemented for slope stabilization and water harvesting are widespread on the slopes of the intramountainous basins and along the slopes of the Bakırçay and Madra tributaries; today they are preferably used for olive groves [44,110] (Figure S6). Ancient agricultural terraces from the Aegean Region date to at least Greco-Roman times [125,126].

## 6. Conclusions

The Bakırçay and Madra River catchments and adjacent coastal areas form major parts of the Pergamon Micro-Region, corresponding to the environs of the UNESCO World Heritage site of Pergamon (modern Bergama). The landform characteristic of this area is highly influenced by tectonic processes and structural components. Overall, the Pergamon Micro-Region is an impressive example of a complex morphotectonic landscape, attributed to interfingering factors of tectonics, lithology, sea-level change, and human impact on erosion and sedimentation processes. Cenozoic tectonics and volcanism formed the basic horst and graben structures. Plio-Pleistocene tensional forces and crustal stretching formed the Bergama Graben and the adjoining horsts with their intramountainous basins. The Kozak Mountains to the north of the lower Bakırçay plain, and the Yunt Dağı Mountains to its south, show remarkably asymmetrical geomorphological features, displaying these tectonic influences. The continuous uplift of the Kozak Horst resulted locally in a mountainous relief. Extensive interior plains served as local sediment sinks, which vary in size within highland areas. Rich mineral resources, such as coal, gold and silver, and perlite, are present and have been continuously mined since antiquity, forming extensive quarrying areas. Overall, Quaternary tectonics resulted in a widely immature relief, which remains highly dynamic in the present day.

Due to the availability of several natural resources, the Pergamon Micro-Region was a preferred settlement area in early times. The infills of the intramountainous basins and graben structures provide suitable grounds for agriculture. Perennial streams sourced in the adjoining mountainous areas provide year-round water. Widespread andesitic rocks are an appropriate construction material. The forest areas in the adjoining mountains provided sufficient amounts of wood for construction needs and charcoal production. The topography of the Bergama Graben is characterized by two small seaside accesses and the potentially flood-safe footslopes of the adjoining graben flanks, thus providing a high degree of protection for the settlements on the Bakırçay plain. However, as early as during antiquity, unsuitable land use triggered an enhancement in morphodynamics, resulting in extended colluvial deposition and an increase in the major river sediment load, causing an aggradation of the alluvial plains and a progression of the delta areas, and finally the silting up of the Elaia harbor area.

**Supplementary Materials:** The following are available online at https://www.mdpi.com/article/10.3390/land10070667/s1. **Table S1:** The definition and classification rules of landform units for the geomorphological map (modified from [83]). **Figure S1:** Çalıbahçe basin, indicating how we use the satellite images and geomorphons to generate the geomorphological map (ridge, valley without fluvial deposits, valley with fluvial deposits and slope with debris cover) and the validation in the field. (A) Data: Google Earth satellite images (WorldView-2, last accessed 8 June 2020). (B) Geomorphological map (legend refers to Figure 4, same below). (C) Landscape photograph. **Figure S2:** Terrace examples: continuous (a) and discontinuous (b). Data: Google Earth satellite images (WorldView-2, last accessed 8 June 2020). **Figure S3:** Slope with bare rock in Tekkedere valley. (A) Data: Google Earth satellite images (WorldView-2, last accessed 8 June 2020). (B) Landscape photograph. **Figure S4:** (A) An example of mining fields and decomposed granite boulders at the northwestern slopes of the Kozak interior plain (subunit 2.1). Data: Google Earth satellite images (WorldView-2, last accessed 8 June 2020). Photographs of a canal on the Bergama Fan (B), slope with debris cover in the Tekkedere valley (C), artificial terraces in Çalıbahçe basin (D), Kısrakdere Coal Mine (E). **Figure S5:** The western lower Bakırçay plain from the Sultantepe to the Yunt Dağı Mountains. (A) The hillshade of TanDEM-X data, indicating the features of alluvial plain and paleochannels which are highlighted in Figure S5: B. (B) Geomorphological map. (C) Landscape photograph. **Figure S6:** The land cover map of the Bakırçay and Madra River catchments and the adjacent coastal areas. Data: Corine Land Cover (CLC) 2018 (Version 2020_20u1) [81]. **Figure S7:** Additional geomorphometric parameter maps derived from TanDEM-X data. (A) Aspect. (B) Topographic Position Index (TPI). (C) Topographic Wetness Index (TWI).

**Author Contributions:** Conceptualization, X.Y., F.B., D.K. and B.S.; methodology, X.Y.; software, X.Y.; validation, X.Y., F.B., D.K. and B.S.; formal analysis, X.Y.; investigation, X.Y., F.B., D.K. and B.S.; resources, D.K.; data curation, X.Y.; writing—original draft preparation, X.Y. and B.S.; writing—review and editing, F.B., D.K. and B.S.; visualization, X.Y. and D.K.; supervision, B.S.; project administration, F.B. and B.S.; funding acquisition, B.S. and D.K. All authors have read and agreed to the published version of the manuscript.

**Funding:** This research was funded by China Scholarship Council (grant number 201906190216) and Deutsche Forschungsgemeinschaft (German Research Foundation; grant number 419349690).

**Acknowledgments:** We thank Murat Tozan for his help during the field work. We are grateful to the anonymous reviewers whose comments helped to improve this paper and two English editors (Christopher Dacosta and Mark Walton). The research was conducted within the project *Die Transformation der Mikroregion Pergamon zwischen Hellenismus und römischer Kaiserzeit* (The Transformation of the Micro-region Pergamon between the Hellenistic Period and the Roman Imperial Age). We acknowledge support by the Open Access Publication Fund of the Freie Universität Berlin.

**Conflicts of Interest:** The authors declare no conflict of interest. The funders had no role in the design of the study; in the collection, analyses, or interpretation of data; in the writing of the manuscript, or in the decision to publish the results.

## References


1. Kayan, İ. Holocene stratigraphy and geomorphological evolution of the Aegean coastal plains of Anatolia. *Quat. Sci. Rev.* **1999**, *18*, 541–548. [CrossRef]
2. Kayan, İ.; Vardar, S. Geomorphological formation and development of the delta plain of the Madra River. In *The Madra River Delta: Regional Studies on the Aegean Coast of Turkey 1: Environment, Society and Community from Prehistory to the Present*; Lambrianides, K., Spencer, N., Eds.; The British Institute at Ankara: London, UK, 2007; Volume 35, pp. 23–30.
3. Kuzucuoğlu, C.; Çiner, A.; Kazancı, N. (Eds.) The Geomorphological Regions of Turkey. In *Landscapes and Landforms of Turkey*; Springer: Cham, Switzerland, 2019; pp. 41–178.
4. Kraft, J.C.; Kayan, İ.; Erol, O. Geomorphic Reconstructions in the Environs of Ancient Troy. *Science* **1980**, *209*, 776–782. [CrossRef]
5. Kayan, İ. Bronze Age Regression and Change of Sedimentation on The Aegean Coastal Plains of Anatolia (Turkey). In *Third Millennium BC Climate Change and Old World Collapse*; Dalfes, H.N., Kukla, G., Weiss, H., Eds.; Springer: Berlin/Heidelberg, Germany, 1997; Volume 49, pp. 431–450.
6. Kraft, J.C.; Rapp, G.; Kayan, İ.; Luce, J.V. Harbor areas at ancient Troy: Sedimentology and geomorphology complement Homer's Iliad. *Geology* **2003**, *31*, 163–166. [CrossRef]
7. Kayan, İ. Landscape Development and Changing Environment of Troia (North-western Anatolia). In *Landscapes and Landforms of Turkey*; Kuzucuoğlu, C., Çiner, A., Kazancı, N., Eds.; Springer: Cham, Switzerland, 2019; pp. 277–291.
8. Schneider, S.; Nykamp, M.; Matthaei, A.; Bebermeier, W.; Schütt, B. Alluvial geoarchaeology of a small drainage basin in western Anatolia: Late Holocene landscape development and the question of the mouth of the Paleo-Bakırçay. *Quat. Int.* **2013**, *312*, 84–95. [CrossRef]
9. Schneider, S.; Matthaei, A.; Bebermeier, W.; Schütt, B. Late Holocene human–environmental interactions in the Eastern Mediterranean: Settlement history and paleogeography of an ancient Aegean hill-top settlement. *Quat. Int.* **2014**, *324*, 84–98. [CrossRef]
10. Schneider, S.; Matthaei, A.; Schlöffel, M.; Meyer, C.; Kronwald, M.; Pint, A.; Schütt, B. A geoarchaeological case study in the chora of Pergamon, western Turkey, to reconstruct the late Holocene landscape development and settlement history. *Quat. Int.* **2015**, *367*, 62–76. [CrossRef]
11. Schneider, S.; Schlöffel, M.; Schwall, C.; Horejs, B.; Schütt, B. First stratigraphic evidence and absolute dating of a Bronze Age settlement in the Bakırçay valley in western Turkey. *J. Archaeol. Sci. Rep.* **2017**, *12*, 316–322. [CrossRef]
12. Knitter, D.; Blum, H.; Horejs, B.; Nakoinz, O.; Schütt, B.; Meyer, M. Integrated centrality analysis: A diachronic comparison of selected Western Anatolian locations. *Quat. Int.* **2013**, *312*, 45–56. [CrossRef]
13. Kraft, J.C.; Bückner, H.; Kayan, İ.; Engelmann, H. The geographies of Ancient Ephesus and the Artemision in Anatolia. *Geoarchaeology* **2007**, *22*, 121–149. [CrossRef]
14. Kraft, J.C.; Rapp, G.; Brükner, H.; Kayan, İ. Results of the struggle at ancient Ephesus: Natural processes 1, human intervention 0. *Geol. Soc. Lond. Spec. Publ.* **2011**, *352*, 27–36. [CrossRef]
15. Stock, F.; Pint, A.; Horejs, B.; Ladstätter, S.; Brückner, H. In search of the harbours: New evidence of Late Roman and Byzantine harbours of Ephesus. *Quat. Int.* **2013**, *312*, 57–69. [CrossRef]
16. Brückner, H.; Müllenhoff, M.; Gehrels, R.; Herda, A.; Knipping, M.; Vött, A. From Archipelago to Floodplain–Geographical and Ecological Changes in Miletus and its Environs During the Last Six Millennia (Western Anatolia, Turkey). *Z. Geomorphol.* **2006**, *142*, 63–83.
17. Ludwig, B. Reconstructing the Ancient Route Network in Pergamon's Surroundings. *Land* **2020**, *9*, 241. [CrossRef]
18. Knitter, D. Central Places and the Environment. Investigations of an Interdependent Relationship. Doctoral Thesis, Freie Universität Berlin, Berlin, Germany, 2013.
19. Horejs, B. Bergama and the Bakırçay Valley in Prehistory. In *Proceedings of International Bergama Symposium*; Önen, E., Mutluer, M., Çetin, N., Eds.; Bergama Belediyesi: Bergama, İzmir, 2011; pp. 24–36.
20. Radt, W. *Pergamon: Geschichte und Bauten Einer Antiken Metropol*; Primus Verlag: Darmstadt, Germany, 2016.
21. Yilmaz, H.; Oyman, T.; Arehart, G.B.; Colakoglu, A.R.; Billor, Z. Low-sulfidation type Au–Ag mineralization at Bergama, Izmir, Turkey. *Ore Geol. Rev.* **2007**, *32*, 81–124. [CrossRef]
22. Russell, B. *Gazetteer of Stone Quarries in the Roman World*; Version 1.0; Oxford University Press: Oxford, UK, 2013; p. 6. Available online: Oxrep.classics.ox.ac.uk/databases/stone_quarries_database/ (accessed on 20 December 2020).
23. Rizzoli, P.; Martone, M.; Gonzalez, C.; Wecklich, C.; Borla Tridon, D.; Bräutigam, B.; Bachmann, M.; Schulze, D.; Fritz, T.; Huber, M.; et al. Generation and performance assessment of the global TanDEM-X digital elevation model. *ISPRS J. Photogramm. Remote Sens.* **2017**, *132*, 119–139. [CrossRef]
24. Wessel, B.; Huber, M.; Wohlfart, C.; Marschalk, U.; Kosmann, D.; Roth, A. Accuracy assessment of the global TanDEM-X Digital Elevation Model with GPS data. *ISPRS J. Photogramm. Remote Sens.* **2018**, *139*, 171–182. [CrossRef]
25. Okay, A. Geology of Turkey: A Synopsis. *Anschitt* **2008**, *21*, 19–42.
26. Pavúk, P.; Horejs, B. Ceramics, Surveys, and Connectivity in Western Anatolia: The Middle and Late Bronze Age Bakirçay/Kaikos Valley Restudied. *Ägypten Levante* **2018**, 457–485. [CrossRef]
27. Pirson, F. Stadt und Umland von Pergamon. Stand der Forschung und Perspektiven. In *Anatolien—Brücke der Kulturen*; Yalçın, Ü., Bienert, H.D., Eds.; Bochum: Bonn, Germany, 2015; pp. 289–310.
28. Laabs, J.; Knitter, D. How Much Is Enough? First Steps to a Social Ecology of the Pergamon Microregion. *Land* **2021**, *10*, 479. [CrossRef]

29. Lolling, H. Atarneus. *Mitt. Dtsch. Archäol. Inst. Athen. Abt.* **1879**, *4*, 1–10.
30. Philippson, A. Geographisch-geologische Übersicht der Landschaft. In *Altertümer von Pergamon: Stadt und Landschaft*; Conze, A., Ed.; Verlag von Georg Reimer: Berlin, Germany, 1912; pp. 43–58.
31. Pirson, F.; Horejs, B.; Laufer, E.; Schwall, C.; Schwarz, A.J. Pergamon—Bericht über die Arbeiten in der Kampagne 2015. *Archäol. Anz.* **2016**, *2*, 135–223.
32. Horejs, B. Bronzezeitliche Besiedlungsmuster im Kaikostal. Interpretationen erster Surveyergebnisse im Umland von Pergamon (Türkei). In *Siedlung und Handwerk—Studien zu Sozialen Kontexten in der Bronzezeit*; Horejs, B., Kienlin, T.L., Eds.; Verlag Dr. Rudolf Habelt: Bonn, Germany, 2010; Volume 194, pp. 47–67.
33. Sommerey, K.M. Die Chora von Pergamon: Studien zu Grenzen, Siedlungsstruktur und Wirtschaft. In *Istanbuler Mitteilungen*; Pirson, F., Bachmann, M., Eds.; Ernst Wasmuth: Tübingen, Germany, 2008; Volume 58, pp. 135–170.
34. Kökten, K. 1949 yılı tarih öncesi araştırmaları hakkında kısa rapor. *Belleten* **1949**, *13*, 811–831.
35. Pint, A.; Seeliger, M.; Frenzel, P.; Feuser, S.; Erkul, E.; Berndt, C.; Klein, C.; Pirson, F.; Brückner, H. The environs of Elaia's ancient open harbour—A reconstruction based on microfaunal evidence. *J. Archaeol. Sci.* **2015**, *54*, 340–355. [CrossRef]
36. Seeliger, M.; Bartz, M.; Erkul, E.; Feuser, S.; Kelterbaum, D.; Klein, C.; Pirson, F.; Vött, A.; Brückner, H. Taken from the sea, reclaimed by the sea: The fate of the closed harbour of Elaia, the maritime satellite city of Pergamum (Turkey). *Quat. Int.* **2013**, *312*, 70–83. [CrossRef]
37. Seeliger, M.; Brill, D.; Feuser, S.; Bartz, M.; Erkul, E.; Kelterbaum, D.; Vött, A.; Klein, C.; Pirson, F.; Brückner, H. The Purpose and Age of Underwater Walls in the Bay of Elaia of Western Turkey: A Multidisciplinary Approach. *Geoarchaeology* **2014**, *29*, 138–155. [CrossRef]
38. Seeliger, M.; Pint, A.; Feuser, S.; Riedesel, S.; Marriner, N.; Frenzel, P.; Pirson, F.; Bolten, A.; Brückner, H. Elaia, Pergamon's maritime satellite: The rise and fall of an ancient harbour city shaped by shoreline migration. *J. Quat. Sci.* **2019**, *34*, 228–244. [CrossRef]
39. Seeliger, M.; Pint, A.; Frenzel, P.; Feuser, S.; Pirson, F.; Riedesel, S.; Brückner, H. Foraminifera as markers of Holocene sea-level fluctuations and water depths of ancient harbours—A case study from the Bay of Elaia (W Turkey). *Palaeogeogr. Palaeoclimatol. Palaeoecol.* **2017**, *482*, 17–29. [CrossRef]
40. Shumilovskikh, L.S.; Seeliger, M.; Feuser, S.; Novenko, E.; Schlütz, F.; Pint, A.; Pirson, F.; Brückner, H. The harbour of Elaia: A palynological archive for human environmental interactions during the last 7500 years. *Quat. Sci. Rev.* **2016**, *149*, 167–187. [CrossRef]
41. Mecking, R.; Meinecke, M.; Erkul, E.; Driehaus, B.; Bolten, A.; Pirson, F.; Rabbel, W. The Yığma Tepe of Pergamon: Stratigraphic construction of a monumental tumulus from seismic refraction measurements. *Archaeol. Prospect.* **2020**, *27*, 73–105. [CrossRef]
42. Becker, F.; Knitter, D.; Nykamp, M.; Schütt, B. Meta-Analysis of Geomorphodynamics in the Western Lower Bakırçay Plain (Aegean Region, Turkey). *Land* **2020**, *9*, 338. [CrossRef]
43. Lambrianides, K.; Spencer, N. *The Madra River Delta: Regional Studies on the Aegean Coast of Turkey 1: Environment, Society and Community from Prehistory to the Present*; The British Institute at Ankara: London, UK, 2007; Volume 35.
44. Pirson, F. Pergamon—Bericht über die Arbeiten in der Kampagne 2018. *Archäol. Anz.* **2019**, *2*, 1–157. [CrossRef]
45. Yilmaz, Y.; Genç, Ş.C.; Gürer, F.; Bozcu, M.; Yilmaz, K.; Karacik, Z.; Altunkaynak, Ş.; Elmas, A. When did the western Anatolian grabens begin to develop? In *Tectonics and Magmatism in Turkey and the Surrounding Area*; Bozkurt, E., Winchester, J.A., Piper, J.D.A., Eds.; Geological Society of London: London, UK, 2000; Volume 173, pp. 353–384.
46. İnci, U. Depositional evolution of Miocene coal successions in the Soma coalfield, western Turkey. *Int. J. Coal Geol.* **2002**, *51*, 1–29. [CrossRef]
47. Kaya, O.; Ünay, E.n.; Göktaş, F.k.; Saraç, G. Early Miocene stratigraphy of central west Anatolia, Turkey: Implications for the tectonic evolution of the eastern Aegean area. *Geol. J.* **2007**, *42*, 85–109. [CrossRef]
48. Sanğu, E.; Gürer, Ö.F.; Gürer, A. Fault kinematic and Plio-Quaternary paleostress evolution of the Bakırçay Basin, Western Turkey. *Int. Geol. Rev.* **2020**, *62*, 1245–1261. [CrossRef]
49. Karacik, Z.; Yilmaz, Y.; Pearce, J. The Dikili-Çandarlı Volcanics, Western Turkey: Magmatic Interactions as Recorded by Petrographic and Geochemical Features. *Turk. J. Earth Sci.* **2007**, *16*, 493–522.
50. Borsi, S.; Ferrara, G.; Innocenti, F.; Mazzuoli, R. Geochronology and petrology of recent volcanics in the eastern Aegean Sea (West Anatolia and Lesvos Island). *Bull. Volcanol.* **1972**, *36*, 473–496. [CrossRef]
51. Kuzucuoğlu, C. River response to Quaternary tectonics with examples from northwestern Anatolia, Turkey. In *Mediterranean Quaternary River Environments*; Lewin, J., Macklin, M.G., Woodward, J.C., Eds.; Balkema: Rotterdam, The Netherlands, 1995; pp. 45–53.
52. Baartman, J.; Masselink, R.; Keesstra, S.; Temme, A. Linking landscape morphological complexity and sediment connectivity. *Earth Surf. Process. Landf.* **2013**, *38*, 1457–1471. [CrossRef]
53. Fryirs, K.A.; Brierley, G.J.; Preston, N.J.; Kasai, M. Buffers, barriers and blankets: The (dis)connectivity of catchment-scale sediment cascades. *Catena* **2007**, *70*, 49–67. [CrossRef]
54. Fryirs, K. (Dis)Connectivity in catchment sediment cascades: A fresh look at the sediment delivery problem. *Earth Surf. Process. Landf.* **2013**, *38*, 30–46. [CrossRef]
55. Finné, M.; Woodbridge, J.; Labuhn, I.; Roberts, C.N. Holocene hydro-climatic variability in the Mediterranean: A synthetic multi-proxy reconstruction. *Holocene* **2019**, *29*, 847–863. [CrossRef]

56. Dusar, B.; Verstraeten, G.; Notebaert, B.; Bakker, J. Holocene environmental change and its impact on sediment dynamics in the Eastern Mediterranean. *Earth Sci. Rev.* **2011**, *108*, 137–157. [CrossRef]
57. Roberts, C.N.; Woodbridge, J.; Palmisano, A.; Bevan, A.; Fyfe, R.; Shennan, S. Mediterranean landscape change during the Holocene: Synthesis, comparison and regional trends in population, land cover and climate. *Holocene* **2019**, *29*, 923–937. [CrossRef]
58. Tassios, T.P. Water supply of ancient Greek cities. *Water Supply* **2007**, *7*, 165–172. [CrossRef]
59. Macklin, M.; Lewin, J.; Woodward, J. (Eds.) Quaternary fluvial systems in the Mediterranean basin. In *Mediterranean Quaternary River Environments*; Balkema: Rotterdam, The Netherlands, 1995; pp. 1–25.
60. MTA. *Geological Map of Turkey, 1:500,000 (İzmir)*; General Directorate of Mineral Research and Exploration: Ankara, Turkey, 2002.
61. Aksu, A.E.; Piper, D.J.W.; Konuk, T. Late Quaternary tectonic and sedimentary history of outer Izmir and Candarli bays, western Turkey. *Mar. Geol.* **1987**, *76*, 89–104. [CrossRef]
62. Kayan, İ. Late Holocene sea-level changes on the western Anatolian coast. *Palaeogeogr. Palaeoclimatol. Palaeoecol.* **1988**, *68*, 205–218. [CrossRef]
63. Aksu, A.E.; Konuk, T.; Uluğ, A.; Duman, M.; Piper, D.J.W. Quaternary tectonic and sedimentary history of eastern Aegean Sea shelf area. *Jeofizik* **1990**, *4*, 3–35.
64. Vacchi, M.; Rovere, A.; Chatzipetros, A.; Zouros, N.; Firpo, M. An updated database of Holocene relative sea level changes in NE Aegean Sea. *Quat. Int.* **2014**, *328–329*, 301–310. [CrossRef]
65. Kuzucuoğlu, C.; Celâl Şengör, A.M.; Çiner, A. The Tectonic Control on the Geomorphological Landscapes of Turkey. In *Landscapes and Landforms of Turkey*; Kuzucuoğlu, C., Çiner, A., Kazancı, N., Eds.; Springer: Cham, Switzerland, 2019; pp. 17–40.
66. Altunkaynak, Ş.; Yılmaz, Y. The Mount Kozak magmatic complex, Western Anatolia. *J. Volcanol. Geotherm. Res.* **1998**, *85*, 211–231. [CrossRef]
67. Emre, Ö.; Özalp, S.; Dogan, A.; Özaksoy, V.; Yildirim, C.; Göktas, F. *Izmir Yakın Çevresinin diri Fayları ve Deprem Potansiyelleri (Active Faults and Earthquake Potential in the Izmir Region)*; General Directorate of Mineral Research and Exploration (MTA Rapor No: 10754): Ankara, Turkey, 2005.
68. Paradisopoulou, P.M.; Papadimitriou, E.E.; Karakostas, V.G.; Taymaz, T.; Kilias, A.; Yolsal, S. Seismic Hazard Evaluation in Western Turkey as Revealed by Stress Transfer and Time-dependent Probability Calculations. *Pure Appl. Geophys.* **2010**, *167*, 1013–1048. [CrossRef]
69. Emre, Ö.; Doğan, A. *1:250,000 Scale Active Fault Map Series of Turkey, Ayvalık (NJ 35-2) Quadrangle*; Serial Number: 2; General Directorate of Mineral Research and Exploration: Ankara, Turkey, 2010.
70. Emre, Ö.; Doğan, A.; Özalp, S. *1:250,000 Scale Active Fault Map Series of Turkey, Balıkesir (NJ 35-3) Quadrangle*; Serial Number: 4; General Directorate of Mineral Research and Exploration: Ankara, Turkey, 2011.
71. Emre, Ö.; Özalp, S. *1:250,000 Scale Active Fault Map Series of Turkey, Urla (NJ 35-6) Quadrangle*; Serial Number: 5; General Directorate of Mineral Research and Exploration: Ankara, Turkey, 2011.
72. Emre, Ö.; Özalp, S.; Duman, T.Y. *1:250,000 Scale Active Fault Map Series of Turkey, İzmir (NJ 35-7) Quadrangle*; Serial Number: 6; General Directorate of Mineral Research and Exploration: Ankara, Turkey, 2011.
73. Ölgen, K. Determining lineaments and geomorphic features using Landsat 5-TM data on lower Bakırçay plain, Western Turkey. *Aegean Geogr. J.* **2004**, *13*, 47–57.
74. Erlat, E. Climatic conditions in Altınova and the Madra River Delta. In *The Madra River Delta: Regional Studies on the Aegean Coast of Turkey 1: Environment, Society and Community from Prehistory to the Present*; Lambrianides, K., Spencer, N., Eds.; The British Institute at Ankara: London, UK, 2007; Volume 35, pp. 51–59.
75. Danacıoğlu, S.; Tağıl, Ş. Evaluation of the erosion risk by using the RUSLE model in Bakırçay basin. *Balıkesir Üniv. Sos. Bilim. Enst. Derg.* **2017**, *20*, 1–18. (In Turkish)
76. Kapur, S.; Akça, E.; Günal, H. *The Soils of Turkey*; Springer: Cham, Switzerland, 2017.
77. Akman, Y.; Ketenoğlu, O. The climate and vegetation of Turkey. *Proc. R. Soc. Edinb.* **1986**, *89B*, 123–134. [CrossRef]
78. Peel, M.C.; Finlayson, B.L.; McMahon, T.A. Updated world map of the Köppen-Geiger climate classification. *Hydrol. Earth Syst. Sci.* **2007**, *11*, 1633–1644. [CrossRef]
79. Harris, I.; Jones, P.D.; Osborn, T.J.; Lister, D.H. Updated high-resolution grids of monthly climatic observations—The CRU TS3.10 Dataset. *Int. J. Climatol.* **2014**, *34*, 623–642. [CrossRef]
80. Rohling, E.J.; Marino, G.; Grant, K.M.; Mayewski, P.A.; Weninger, B. A model for archaeologically relevant Holocene climate impacts in the Aegean-Levantine region (easternmost Mediterranean). *Quat. Sci. Rev.* **2019**, *208*, 38–53. [CrossRef]
81. Cole, B.; Smith, G.; Balzter, H. Acceleration and fragmentation of CORINE land cover changes in the United Kingdom from 2006–2012 detected by Copernicus IMAGE2012 satellite data. *Int. J. Appl. Earth Obs. Geoinf.* **2018**, *73*, 107–122. [CrossRef]
82. QGIS Development Team. *QGIS Geographic Information System*; Open Source Geospatial Foundation Project: Beaverton, OR, USA, 2020.
83. Walstra, J.; Heyvaert, V.; Verkinderen, P. Remote sensing for the study of fluvial landscapes in Lower Khuzestan, SW Iran. In *Developments in Earth Surface Processes*; Elsevier: Leicester, UK, 2009; Volume 15.
84. Hengl, T.; Reuter, H.I. Geomorphometry—Concepts, Software, Applications. In *Developments in Soil Science*; Hartemink, A.E., McBratney, A.B., Eds.; Elsevier: Amsterdam, The Netherlands, 2009; Volume 33, pp. 1–796.
85. GRASS Development Team. *Geographic Resources Analysis Support System (GRASS) Software*; Version 7.8; Open Source Geospatial Foundation: Beaverton, OR, USA, 2020.

86. Conrad, O.; Bechtel, B.; Bock, M.; Dietrich, H.; Fischer, E.; Gerlitz, L.; Wehberg, J.; Wichmann, V.; Böhner, J. System for Automated Geoscientific Analyses (SAGA) v. 2.1.4. *Geosci. Model Dev.* **2015**, *8*, 1991–2007. [CrossRef]
87. Hofierka, J.; Mitasova, H.; Neteler, M. Geomorphometry in GRASS GIS. In *Geomorphometry: Concepts, Software, Applications. Developments in Soil Science*; Hengl, T., Reuter, H.I., Eds.; Elsevier: Amsterdam, The Netherlands, 2009; Volume 33, pp. 387–410.
88. Jasiewicz, J.; Stepinski, T.F. Geomorphons—A pattern recognition approach to classification and mapping of landforms. *Geomorphology* **2013**, *182*, 147–156. [CrossRef]
89. Guisan, A.; Weiss, S.B.; Weiss, A.D. GLM versus CCA spatial modeling of plant species distribution. *Plant Ecol.* **1999**, *143*, 107–122. [CrossRef]
90. Weiss, A. *Topographic Position and Landforms Analysis*; ESRI User Conference (Poster Presentation): San Diego, CA, USA, 2001.
91. Beven, K.J.; Kirkby, M.J. A physically based, variable contributing area model of basin hydrology. *Hydrol. Sci. Bull.* **1979**, *24*, 43–69. [CrossRef]
92. Moore, I.D.; Grayson, R.B.; Ladson, A.R. Digital Terrain Modeling: A Review of Hydrological, Geomorphological, and Biological Applications. *Hydrol. Process.* **1991**, *5*, 3–30. [CrossRef]
93. Mattivi, P.; Franci, F.; Lambertini, A.; Bitelli, G. TWI computation: A comparison of different open source GISs. *Open Geospat. Data Softw. Stand.* **2019**, *4*, 6. [CrossRef]
94. Rhoads, B.L. *River Dynamics: Geomorphology to Support Management*; Cambridge University Press: Cambridge, UK, 2020.
95. Mahmood, S.A.; Gloaguen, R. Appraisal of active tectonics in Hindu Kush: Insights from DEM derived geomorphic indices and drainage analysis. *Geosci. Front.* **2012**, *3*, 407–428. [CrossRef]
96. Bull, W.B. *Tectonic Geomorphology of Mountains: A New Approach to Paleoseismology*; Wiley-Blackwell: Oxford, UK, 2007; pp. 1–328.
97. Telbisz, T.; Kovács, G.; Székely, B.; Szabó, J. Topographic swath profile analysis: A generalization and sensitivity evaluation of a digital terrain analysis tool. *Z. Geomorphol.* **2013**, *57*, 485–513. [CrossRef]
98. Yilmaz, H.; Oyman, T.; Sönmez, F.N.; Arehart, G.B.; Billor, Z. Intermediate sulfidation epithermal gold-base metal deposits in Tertiary subaerial volcanic rocks, Sahinli/Tespih Dere (Lapseki/Western Turkey). *Ore Geol. Rev.* **2010**, *37*, 236–258. [CrossRef]
99. Tosun, H.; Tosun, T.; Hariri-Ardebili, M. Total risk and seismic hazard analysis of large embankment dams: Case study of Northwest Anatolia, Turkey. *Life Cycle Reliab. Saf. Eng.* **2020**, *9*, 329–338. [CrossRef]
100. Karaoğlu, Ö. Tectonic controls on the Yamanlar volcano and Yuntdağı volcanic region, western Turkey: Implications for an incremental deformation. *J. Volcanol. Geotherm. Res.* **2014**, *274*, 16–33. [CrossRef]
101. Kayan, İ.; Vardar, S. The physical geography of the Madra River Delta. In *The Madra River Delta: Regional Studies on the Aegean Coast of Turkey 1: Environment, Society and Community from Prehistory to the Present*; Lambrianides, K., Spencer, N., Eds.; The British Institute at Ankara: London, UK, 2007; Volume 35, pp. 9–23.
102. Gutiérrez, F.; Gutiérrez, M. (Eds.) Granite Landforms. In *Landforms of the Earth*; Springer: Cham, Switzerland, 2016; pp. 103–109.
103. Mustafaoğlu, G.; Dağ, H.U. Cultural heritage works of the Gebze-İzmir Motorway Project in the west of Turkey. *Eur. Assoc. Archaeol.* **2012**, *38*, 25–30.
104. Lague, D. The stream power river incision model: Evidence, theory and beyond. *Earth Surf. Process. Landf.* **2014**, *39*, 38–61. [CrossRef]
105. Bull, W.B. The alluvial-fan environment. *Prog. Phys. Geogr. Earth Environ.* **1977**, *1*, 222–270. [CrossRef]
106. Clarke, L.E. Experimental alluvial fans: Advances in understanding of fan dynamics and processes. *Geomorphology* **2015**, *244*, 135–145. [CrossRef]
107. Ahnert, F. Functional relationships between denudation, relief, and uplift in large, mid-latitude drainage basins. *Am. J. Sci.* **1970**, *268*, 243. [CrossRef]
108. Schlunegger, F.; Hinderer, M. Pleistocene/Holocene climate change, re-establishment of fluvial drainage network and increase in relief in the Swiss Alps. *Terra Nova* **2003**, *15*, 88–95. [CrossRef]
109. Das, S. Geomorphic characteristics of a bedrock river inferred from drainage quantification, longitudinal profile, knickzone identification and concavity analysis: A DEM-based study. *Arab. J. Geosci.* **2018**, *11*, 680. [CrossRef]
110. Pirson, F. Pergamon—Das neue Forschungsprogramm und die Arbeiten in der Kampagne 2019. *Archäol. Anz.* **2020**, *2*, 1–245. [CrossRef]
111. Ozdemir, H.; Bird, D. Evaluation of morphometric parameters of drainage networks derived from topographic maps and DEM in point of floods. *Environ. Geol.* **2008**, *56*, 1405–1415. [CrossRef]
112. Bagha, N.; Arian, M.; Ghorashi, M.; Pourkermani, M.; El Hamdouni, R.; Solgi, A. Evaluation of relative tectonic activity in the Tehran basin, central Alborz, northern Iran. *Geomorphology* **2014**, *213*, 66–87. [CrossRef]
113. Özürlan, G.; Candansayar, M.E.; Şahin, M.H. Deep resistivity structure of the Dikili-Bergama region, west Anatolia, revealed by two- dimensional inversion of vertical electrical sounding data. *Geophys. Prospect.* **2006**, *54*, 187–197. [CrossRef]
114. Brückner, H.; Kelterbaum, D.; Marunchak, O.; Porotov, A.; Vött, A. The Holocene sea level story since 7500 BP—Lessons from the Eastern Mediterranean, the Black and the Azov Seas. *Quat. Int.* **2010**, *225*, 160–179. [CrossRef]
115. Marriner, N.; Morhange, C. Geoscience of ancient Mediterranean harbours. *Earth Sci. Rev.* **2007**, *80*, 137–194. [CrossRef]
116. Boyer, P.; Roberts, N.; Baird, D. Holocene environment and settlement on the Çarşamba alluvial fan, south-central Turkey: Integrating geoarchaeology and archaeological field survey. *Geoarchaeology* **2006**, *21*, 675–698. [CrossRef]
117. Von Diest, W. *Von Pergamon Über den Dindymos zum Pontus*; Justus Perthes: Gotha, Germany, 1889.
118. Zimmermann, M. *Pergamon. Geschichte, Kultur, Archäologie*; C.H. Beck: München, Germany, 2011.

119. Schneider, S. Geoarchaeological Case Studies in the Bakırçay Valley—Paleogeography and Human-Environmental Interactions in the Chora of Pergamon in Western Turkey. Doctoral Thesis, Freie Universität Berlin, Berlin, Germany, 2014.
120. Karayiğit, A.İ.; Littke, R.; Querol, X.; Jones, T.; Oskay, R.G.; Christanis, K. The Miocene coal seams in the Soma Basin (W. Turkey): Insights from coal petrography, mineralogy and geochemistry. *Int. J. Coal Geol.* **2017**, *173*, 110–128. [CrossRef]
121. Oskay, R.G.; Bechtel, A.; Karayiğit, A.İ. Mineralogy, petrography and organic geochemistry of Miocene coal seams in the Kınık coalfield (Soma Basin-Western Turkey): Insights into depositional environment and palaeovegetation. *Int. J. Coal Geol.* **2019**, *210*, 103205. [CrossRef]
122. Dill, H.G.; Dohrmann, R.; Kaufhold, S.; Çiçek, G. Mineralogical, chemical and micromorphological studies of the argillic alteration zone of the epithermal gold deposit Ovacik, Western Turkey: Tools for applied and genetic economic geology. *J. Geochem. Explor.* **2015**, *148*, 105–127. [CrossRef]
123. Russell, B. *The Economics of the Roman Stone Trade*; Oxford University Press: Oxford, UK, 2013; pp. 87–88.
124. Hökerek, S.; Özçelik, O. Organic Facies Characteristics of the Miocene Soma Formation (Lower Lignite Succession-KM2), Soma Coal Basin, Western Turkey. *Energy Procedia* **2015**, *76*, 27–32. [CrossRef]
125. Grove, A.T.; Rackham, O. *The Nature of Mediterranean Europe: An Ecological History*; Yale University Press: New Haven, CT, USA, 2003.
126. Price, S.; Nixon, L. Ancient Greek Agricultural Terraces: Evidence from Texts and Archaeological Survey. *Am. J. Archaeol.* **2005**, *109*, 665–694. [CrossRef]